Review

Uranium Removal from Aqueous Solutions by Aerogel-Based Adsorbents – A critical review

Efthalia Georgiou [1], Grigorios Raptopoulos [2], Ioannis Anastopoulos [3], Dimitrios A. Giannakoudakis [4], Michael Arkas [5,*], Patrina Paraskevopoulou [2,*], Ioannis Pashalidis [1]

[1] Radioanalytical and Environmental Chemistry Group, Department of Chemistry, University of Cyprus, P.O. Box 20537, Nicosia, CY-1678, Cyprus.; georgiou.efthalia@ucy.ac.cy (E.G.); pspasch@ucy.ac.cy (I.P.)
[2] Inorganic Chemistry Laboratory, Department of Chemistry, National and Kapodistrian University of Athens, Panepistimiopolis Zografou, 15771 Athens, Greece; grigorisrap@chem.uoa.gr (G.R.); paraskevopoulou@chem.uoa.gr (P.P.)
[3] Department of Agriculture, University of Ioannina, UoI Kostakii Campus, 47100 Arta, Greece; anastopoulos_ioannis@windowslive.com (I.A.)
[4] Department Chemistry, Aristotle University of Thessaloniki, Thessaloniki, Greece; dagchem@gmail.com (D.G.)
[5] Demokritos National Centre for Scientific Research, Institute of Nanoscience and Nanotechnology, Athens, Greece.; m.arkas@inn.demokritos.gr (M.A.)
* Correspondence: paraskevopoulou@chem.uoa.gr Tel: +30-210-727-4381 (P.P.); m.arkas@inn.demokritos.gr Tel.: +30-210-650-3669 (M.A.)

Abstract: Aerogel-based adsorbents present extraordinary sorption capacity for hexavalent uranium that can be as high as 8.8 mol kg^{-1} (2088 g kg^{-1}). The adsorption data follow generally the *Langmuir* isotherm model and the kinetic data are better described by the pseudo-second-order kinetic model, which is associated with chemisorption. Evaluation of the thermodynamic data reveals that the adsorption is generally an endothermic, entropy-driven process (ΔH^o, $\Delta S^o > 0$). Spectroscopic studies (e.g., FTIR, XPS) indicate that the adsorption is based on the formation of inner-sphere complexes between surface active moieties and the uranyl cation. Regeneration and uranium recovery by acidification and complexation using carbonate or chelating ligands (e.g., EDTA) have been found to be successful. The application of aerogel-based adsorbents to uranium removal from industrial processes and uranium-contaminated waste waters was also successful, assuming that these materials could be very attractive as adsorbents in water treatment and uranium recovery technologies. However, the selectivity of the studied materials towards hexavalent uranium is limited suggesting further development of aerogel materials which could be modified by surface derivatization with chelating agents (e.g., salophen, iminodiacetate) presenting high selectivity for uranyl moieties.

Keywords: aerogels; environmental remediation; uranium adsorption; environmental water decontamination; adsorption thermodynamics and kinetics; extraordinary adsorption capacity; qmax values; competitive ions; material recycling; uranium recovery

1. Introduction

The rapid industrial development and enormous technological progress in the last decades resulted in the accumulation of organic chemicals (e.g., dyes, pesticides, pharmaceuticals etc.), heavy/toxic metals, metalloids and radionuclides, mainly in waste form, polluting the environment and threatening living organisms [1–5]. Pollution related to (radio)toxic metals and metalloids is of particular interest because of their persistence and complex environmental chemistry. Metal/metalloid ions can enter water bodies after dissolution and extraction from solid matrices, or the deposition of airborne particles. Then they can go into the biosphere including larger organisms mainly through the food chain [6,7].

Increased amounts of (radio)toxic metals and particularly uranium have been accumulated in the environment mainly through anthropogenic activities related to mining and ore beneficiation, energy production (e.g., nuclear power), fertilizer production and the use of depleted uranium in armour-piercing ammunition and tank armour. Uranium, an actinide element, is of particular interest not only because of its chemical toxicity but also because it is a radioactive element with its most abundant isotope having a very long half-life ($t_{1/2} = 4.5\times10^9$ years) and emitting high energy alpha-particles (~4.5 MeV) [8,9]. The aqueous chemistry of uranium can be very complex since it can undergo various chemical transformations, such as reduction/oxidation, hydrolysis, complexation, colloid formation, sorption and precipitation, forming a wide spectrum of chemical species, which behave differently in aquatic systems [9–11].

Regarding the removal of uranium from industrial process solutions and contaminated waters a large spectrum of treatment technologies (e.g., ion exchange, precipitation, solvent extraction, adsorption) has been investigated. However, among them, adsorption is the most attractive route. Adsorption is a chemical process that includes a solid phase (adsorbent) and a liquid phase, which contains the soluble species to be adsorbed (adsorbate). The adsorption of uranium, which basically exists in aqueous solutions in its hexavalent form (U(VI)), occurs via pure electrostatic attraction between the oppositely charged surface of the adsorbate and/or via direct binding between surface active groups (e.g., –OH, –COOH) and U(VI) [12–15]. The latter results in the formation of inner-sphere complexes [13,14], whereas the former results mainly in the formation of outer-sphere complexes [16]. Studies on uranium sorption are fundamental and necessary regarding the chemical behaviour and mobility of this (radio)toxic element in the geosphere, the decontamination of waters, and the recovery of this precious metal from industrial processes and wastewater [1,17].

In recent years, investigations are focused on the development and production of very effective and selective adsorbents. Such adsorbent materials include, but are not limited to, inorganic solids (metal oxides and minerals) [18], biomass by-products [12–15], composite materials [19–22], polymers [23,24], dendrimers [25], MOFs [26–28], carbon-based materials [29], hybrid materials [30–32], biopolymer-based materials [33–35]. Recently, and more intensively in the last decade, aerogels of various chemical compositions and nanostructures have been tested for uranium adsorption and recovery from wastewater and seawater, sometimes with impressive performances [36–70]. Aerogels have also been used for the photocatalytic conversion of soluble uranium species to insoluble nanoparticles that can float on water [71] and as hosts of reagents that leach out and cause precipitation of uranium from water [72].

This review presents the recent progress in the development and use of aerogel materials for uranium uptake and recovery from aquatic environments.

1.1. Aerogels

Aerogels have been defined as solid colloidal or polymeric networks expanded throughout their entire volume by a gas [73,74]. In practice, aerogels are nanostructured ultra-lightweight materials [75], consisting mostly of empty space (>80% v/v). They are prepared via sol-gel processes that yield gels, which are subsequently dried by turning the pore-filling solvent into a supercritical fluid and releasing it as a gas (Figure 1). The specific drying process is the key to avoid significant volume reduction or network compaction during the transition from gels to aerogels, and therefore it is still the most widely used, although in some cases materials with aerogel properties have been obtained after sub-critical drying, freeze-drying (cryogels) or even drying under ambient conditions [75].

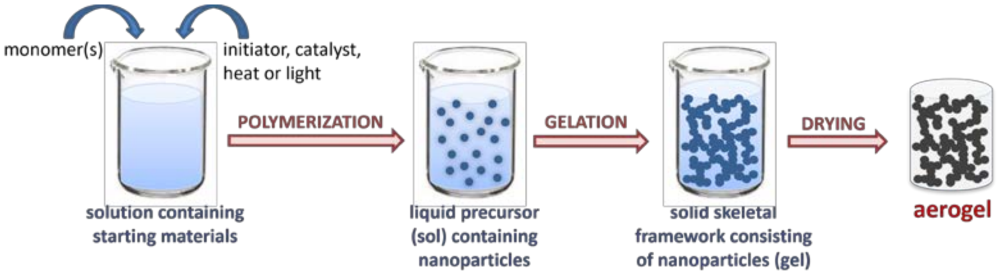

Figure 1. Schematic representation of aerogels synthesis.

S. S. Kistler was the first to prepare silica aerogels, the most well-known type of aerogel, in the 1930s, along with other metal oxide aerogels as well as organic aerogels [76–79]. Kistler’s first silica aerogels were commercialized through Monsanto Chemical Company [80]. Later, in 1966, a new method, using alkoxides as aerogels precursors, was reported by J. B. Peri [81]. From the very first publication by Kistler [76], it was clear that this class of lightweight, nanoporous, nanostructured materials is not limited to a certain chemical composition, not even to a certain class of chemical compounds, but it can include several materials, ranging from inorganic to organic and from synthetic to natural polymers. Indeed, nowadays aerogels are a huge family of materials including inorganic oxides, chalcogenides, metals, ceramics, natural and synthetic organic polymers, and carbons [75,82,83]. In fact, there are no chemical compounds that could not be made in an aerogel form [84]. Aerogels can be prepared in any desirable form factor, including mostly monoliths, but also blankets [85], fibres [86], films [87,88], and millimetre-sized beads or fine powders [89–92].

In addition to the chemical composition, the size and shape of the pores affect the properties of an aerogel, as is the case for all porous materials. Most aerogels are mesoporous materials with pore sizes in the 2–50 nm range. The solid network consists of primary particles that aggregate to form fractal porous secondary particles, eventually agglomerating to a “pearl-necklace” structure. The finely structured porous skeletal framework together with the small size pores provides aerogels with unique properties, among which are higher surface areas, low thermal conductivities, low dielectric constants, and high acoustic attenuation [75]. Interestingly, the nanostructure of the aerogels can be designed and tuned by choosing specific monomers [93–97] or by modifying the synthetic procedure [98–105].

Based on the above, it is obvious that aerogels are extremely versatile and promising materials for a wide range of technological areas. Indeed, IUPAC has recently announced aerogels in the 2022 top ten emerging technologies in Chemistry [106]. The areas of application include, but are not limited to, thermal (their flagship application) [85,107–114] and acoustic insulation [108,109,114], space applications [108,115], transparent materials [116–118] energy storage [99,107,119–121], dielectrics [108], gas and humidity adsorption [108,112,122–125], sensors [114,122], actuators [126–128], catalysis [99,112,122,124,129–133], biomedicine [134,135], the food industry [112,136], environmental remediation [100,134,137,138].

Indeed, the potential of aerogels in the field of environmental remediation is shown by the dramatic increase in the number of publications (Figure 2, left), especially in the last decade, and by the launching in 2019 of a COST Action entitled “Advanced Engineering and Research of aeroGels for Environment and Life Sciences” [139]. Relevant to this review, the number of publications on utilizing aerogels for uranium uptake has been also increasing rapidly in the last decade (Figure 2, right).

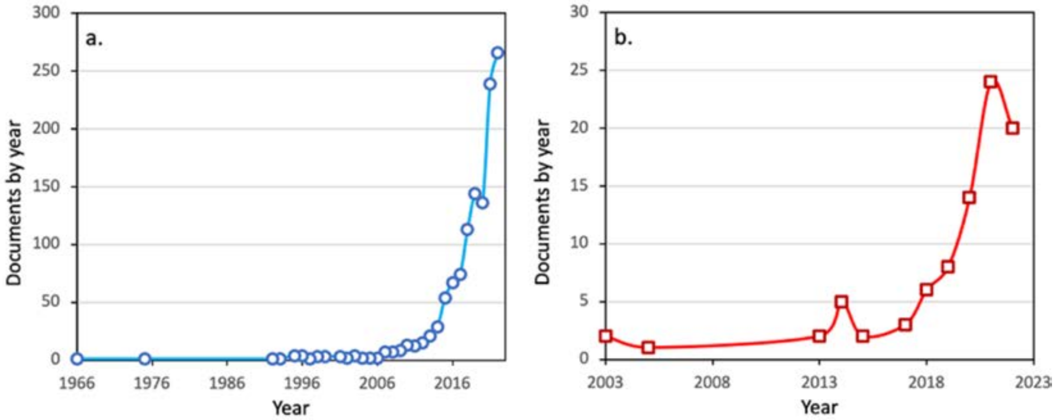

Figure 2. The number of publications on aerogels for environmental applications (left) and aerogels for uranium uptake and recovery (right). Source: Scopus (01.12.2022).

1.2. Uranium

Uranium is a natural element and a member of the actinide series (5*f* elements). It has an atomic number of 92 and an atomic weight of 238.02891 g mol^{-1}. Uranium is a relatively abundant element at a mean concentration of 2.4 ppm in the earth's crust and about 3.3 ppb in the oceans. Natural uranium is a mixture of three isotopes U-238, U-235 and U-234, which is a daughter nuclide of U-238 with a relatively short half-life and hence more or less in radioactive equilibrium with its parent nuclide U-238. All uranium isotopes are alpha-particle-emitting radionuclides, but generally, uranium is a relatively weak radioactive element. However, uranium is a heavy element and hence chemotoxic above certain levels, which are far below the levels of its radiotoxicity [8].

Uranium in nature can exist in five different oxidation states from +2 to +6. However, +4 and +6 are the most abundant oxidation states, and +6 is the predominant oxidation state in aqueous solutions under ambient conditions. In hexavalent oxidation, state uranium exists in the form of the uranyl cation (UO_2^{2+}) and is easily hydrolyzed (pH > 4) in aqueous solutions. The formation of the polynuclear species is favoured at increased U(VI) concentration (> 10^{-5} M). Moreover, under ambient conditions and in the presence of carbonate cations the U(VI) carbonato-species govern the U(VI) chemistry in aqueous solutions and the near neutral and alkaline pH region [10,11,140]. Figure 3 shows the solubility curve of $UO_2(OH)_2$, which is the solubility-limiting solid phase of U(VI) under ambient conditions in aqueous solutions and the corresponding species distribution diagram, which includes only mononuclear U(VI) species. In order to denote the impact of carbonate complexation, Figure 3 includes also the solubility curve of $UO_2(OH)_2$ assuming only hydrolysis. The calculation of both, the solubility curves and the species distribution has been performed using the solubility product of $UO_2(OH)_2$ and the formation constants of the hydrolysis species and carbonate complexes available in the literature [10,11].

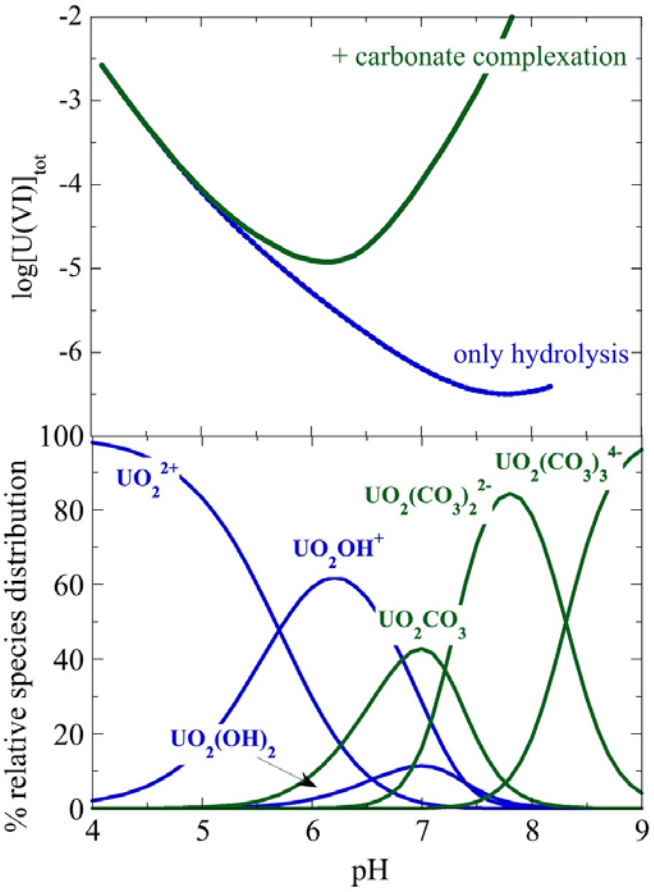

Figure 3. Top: Solubility curve of $UO_2(OH)_2$ assuming only hydrolysis and under ambient conditions hydrolysis and carbonate complexation. Bottom: Speciation diagram including only U(VI) mononuclear species at various pH values.

2. Uranium Sorption by Aerogels

As also stated before, and shown in (Figure 2, right), in recent years a relatively large number of studies has been published regarding the sorption of U(VI) by aerogels and particularly the effect of several parameters (e.g., pH, initial U(VI) concentration, ionic strength, contact time, temperature, adsorbent dosage, presence of competing species) that affect U(VI) sorption. In addition, some of these studies include the possible recovery of uranium and reusability of the aerogel adsorbent, as well as the employment of spectroscopic techniques in order to identify surface species formed after the adsorption and get insight into the sorption mechanism. Table 1 summarizes experimental parameters and thermodynamic data evaluated from published studies on uranium adsorption by several aerogel materials [36–69].

Before we proceed to the analysis of the parameters that affect U(VI) sorption, we need to answer one basic question. How important is the nanostructure of aerogels for the specific application sorption? To answer this question, we will use two examples. First, we will compare the maximum sorption (q_{max}) reported for calcium alginate xerogels (appr. 9 g kg^{-1}) [35] and calcium alginate aerogels (388 g kg^{-1}; Table 1) [38] at pH 3. Since the chemical composition of the adsorbent and the reaction conditions are the same, the huge difference in qmax has to be credited to the nanostructured porous calcium alginate aerogel. Second, we will compare polyurea-crosslinked calcium alginate (X-alginate) aerogels with an aliphatic [141–143] or with an aromatic [144] polyurea. In both cases, the alginate network is covered by polyurea and the materials have similar material properties and morphologies; but there is a critical difference in the nanostructure: the aliphatic polyurea forms a compact layer that covers the alginate primary nanoparticles, while the aromatic polyurea is a more rigid and more randomly oriented polymer structure that partially fills the pores within the secondary particles [94]. Because of this difference, these two materials behave differently versus the sorption of heavy metal ions. X-alginate aerogels with the aromatic polyurea can efficiently uptake Pb(II) [145], U(VI) [38], Eu(III) and Th(IV) [146], while X-alginate aerogels with the aliphatic polyurea are not so efficient. For example, for Pb(II), the q_{max} values are equal to 20.8 g kg^{-1} and 6.8 g kg^{-1}, respectively [147].

Table 1. Selected experimental data for the best-fitted kinetics/isotherm models for the sorption of uranium by aerogel materials.

Aerogel Material	pH	Temp. (K)	$[U(VI)]_0$/max (mol L^{-1})	Best-fitted isotherm/kinetics model	q_{max} (g kg^{-1})	Competition / Recycling / Recovery	Data related to U(VI) adsorption	Ref.
Hydroxyapatite (templated with konjac gum)	4	298	4.2×10^{-4}	*Langmuir*, PSO	2088	anion/cation competition reuse for 5 cycles	FTIR, XPS, mechanistic studies	[36] [37]
Polyurea-crosslinked alginate (X-alginate)	3	298	4.2×10^{-5}	*Langmuir*	2023	natural waters, seawater, modelling, wastewater, recycling	FTIR, EDS	[38]
Reduced graphene oxide/ZIF-67 [a]	4	298	1.05×10^{-3}	*Langmuir*, PSO	1888	cation competition, reuse for 5 cycles	FTIR, XPS	[39]
Al_2O_3/MgO	6	298	4.2×10^{-5}	*Langmuir*, PSO	1047	cation competition, reuse for 5 cycles	XPS, mechanistic studies	[40]
MOF/black phosphorus quantum dots on cellulose [b]	7	303		*Langmuir*, PSO	858	seawater, recycling	XPS, mechanistic studies	[41]
Pr_2O_3	7	298	4.2×10^{-5}	*Langmuir*, PSO	841	cation competition, reuse for 5 cycles	FTIR, XPS	[42]
Al_2O_3 (templated with chitosan)	7	298	4.2×10^{-5}	*Langmuir*, PSO	814	anion/cation competition, reuse for 5 cycles	FTIR, XPS, mechanistic studies	[43] [44]
Al_2O_3 (templated with polyethylene glycol)	7	298	4.2×10^{-5}	*Langmuir*, PSO	737	anion/cation competition, reuse for 5 cycles	FTIR, XPS, mechanistic studies	[43]
Amidoxime-functionalized β-cyclodextrin/graphene	6	298	8.4×10^{-4}	*Langmuir*	654	cation competition, reuse for 10 cycles	FTIR, XPS	[45]
TiO_2	5	298	4.2×10^{-5}	*Langmuir*, PSO	638	cation competition, reuse for 5 cycles	FTIR, XPS	[46]
Al_2O_3 (prepared with thiourea)	7	298	4.2×10^{-5}	*Langmuir*, PSO	634	seawater	FTIR, XPS	[47]
Al_2O_3 (templated with dopamine)	7	298	4.2×10^{-5}	*Langmuir*, PSO	592	anion/cation competition, reuse for 5 cycles	FTIR, XPS, mechanistic studies	[43]
Poly(amidoxime)/graphene oxide nanoribbons	4.5	298	5.0×10^{-4}	*Langmuir*	589	cation competition, reuse for 5 cycles	XPS, mechanistic studies, DFT modelling	[48]
Nd_2O_3	7	-	4.2×10^{-5}	*Langmuir*, PSO	587	cation competition, reuse for 5 cycles	FTIR, XPS	[42]
Bacterial cellulose@ZIF-8 carbon [c]	3	308	8.4×10^{-5}	*Langmuir*, PSO	535	cation competition, reuse for 5 cycles	FTIR, XPS	[49]
Calcium alginate/MgAlFe layered double hydroxides	5	298	8.4×10^{-5}	*Langmuir*, PSO	532	-	FTIR, XPS	[50]
CeO_2	7	298	4.2×10^{-5}	*Langmuir*, PSO	482	cation competition, reuse for 5 cycles	FTIR, XPS	[42]
Nanocellulose	5	298	4.2×10^{-5}	*Langmuir*, PSO	441	cation competition, reuse for 5 cycles	FTIR, XPS	[51]
Chitosan/aluminum sludge composite	4	308	3×10^{-3}	*Langmuir*, PSO	435	cation competition, reuse for 5 cycles	XPS, mechanistic studies	[52]
Graphene oxide nanoribbon	4.5	298	2.52×10^{-4}	*Langmuir*, PSO	431	-		[53]

Calcium alginate	3	298	4.2×10^{-5}	*Langmuir*	388	-		[38]
Iron-polyaniline-graphene composite	5.5	318	4.2×10^{-5}	*Langmuir*, PSO	350	reuse for 5 cycles	FTIR, XPS, EDS mechanistic studies	[54]
Chitosan/carboxylated carbon nanotube composite	5	318	5.04×10^{-4}	*Langmuir*, PSO	341	cation competition	FTIR, XPS	[55]
Bayberry tannin/graphene composite	5	298	-	-	330	-		[56]
Reduced graphene oxide/g-C_3N_4 quantum dots/ZIF-67 composite carbon [a]	3	328	8.4×10^{-5}	*Langmuir*, PSO	316	cation competition, reuse for 5 cycles	FTIR, XPS	[57]
Aromatic polyurea derived from TIPM [d]	3	298	4.2×10^{-5}	*Langmuir*	305	-		[38]
Fungus hypha/graphene oxide	5	293	5.04×10^{-4}	*Langmuir*	288	cation competition, reuse for 6 cycles	XPS	[58]
Aramid/polyamidoxime	6	298	4.2×10^{-4}	*Langmuir*, PSO	262	cation competition, reuse for 5 cycles		[59]
Pr_2O_3	8	298	4.2×10^{-5}	-	252	-		[60]
Graphene	4	298	1.02×10^{-4}	*Langmuir*, PSO	239	reuse for 4 cycles	XPS	[61]
Carbon/Fe_3O_4	6	303	2.1×10^{-4}	*Langmuir*, PSO	230	anion/cation competition, reuse for 5 cycles	FTIR, XPS	[62]
Melamine-formaldehyde/alginate	4	298	4.2×10^{-4}	*Langmuir*	211	cation competition		[63]
Polydopamine- functionalized attapulgite/chitosan	6	-	2.1×10^{-4}	*Langmuir*, PSO	175	reuse for 6 cycles	FTIR, XPS	[64]
p-Phthalaldehyde/3,5-diaminobenzoic acid-crosslinked chitosan	6	308	4.2×10^{-5}	*Langmuir*, PSO	160	-	XPS	[65]
Phosphorylated carbon	5.5	298	4.2×10^{-5}	*Langmuir*, PSO	150	cation competition, reuse for 5 cycles	FTIR, XPS	[66]
Sulfonated graphene	5	298	4.2×10^{-5}	*Langmuir*, PSO	148	cation competition, reuse for 5 cycles	FTIR, XPS	[67]
Graphene oxide/carbon nanotubes	5	298	2.1×10^{-4}	*Langmuir*, PSO	100	-		[68]
Graphene/Ag nanoparticles	5-6	298	8.4×10^{-5}	*Langmuir*	13	-		[69]

[a] ZIF-67: Co-based zeolitic imidazole framework. [b] Under simulated sunlight irradiation. MOF: UiO-66-NH$_2$ (Zr-based metal-organic framework). [c] ZIF-8: Zn-based zeolitic imidazole framework. [d] Aromatic polyurea derived from Desmodur RE (27% w/w triphenylmethane-4,4′,4″-triisocyanate (TIPM) solution in ethyl acetate) from Covestro AG.

2.1. pH Effect

pH is one of the most important parameters regarding sorption since it affects both the speciation of the element in solution and the degree of dissociation of the functional surface groups. Under ambient conditions U(VI) speciation in aqueous solution includes hydrolysis species (e.g., UO_2^{2+}, UO_2OH^{+}, $UO_2(OH)_2$, $(UO_2)_2(OH)_2^{2+}$, $(UO_2)_2OH^{3+}$, $(UO_2)_3(OH)_5^{+}$, $(UO_2)_4(OH)_7^{+}$) which predominate at pH < 6 and U(VI) carbonate complexes (UO_2CO_3, $UO_2(CO_3)_2^{2-}$ and $UO_2(CO_3)_3^{4-}$), which govern the U(VI) chemistry at pH > 6. At pH < 4 the uranyl ion (UO_2^{2+}) dominates and determines the U(VI) chemistry in solution [10].

U(VI) sorption by aerogels has been investigated in a wide pH range (3-11) and the sorption capacity (q_e) has been determined for pH values ranging between 3 and 8, and total U(VI) concentration close or even above the solubility limit of the predominant U(VI) solid phase under ambient conditions (e.g., $UO_2(OH)_2$; Figure 3). This is crucial, particularly in the near neutral pH range (5 < pH < 7) because $UO_2(OH)_2$ is very likely to occur interfering with sorption and resulting in erroneous conclusions. In acidic (pH < 5) and alkaline (pH > 7) solutions the solubility increases significantly due to acidic solid phase dissolution and carbonate complexation of U(VI). It is obvious that studies related to pH-effect should be performed at total U(VI) concentrations below the solubility limits to avoid artifacts associated with solid-phase precipitation. In addition, the formation of hydrolysis and polynuclear species for pH > 4, as well as carbonate complexes for pH > 6 is expected to result in various sorption interactions which may also differ from one aerogel type to another. Therefore, a large variation is observed regarding the pH values at which the maximum sorption capacity (q_{max}) occurs, even for similar types of aerogel materials. In some cases, there is a range of several pH units in which the materials present their q_{max}, while in other cases q_{max} is observed at a certain pH value.

In order to obtain more reliable and comparable results we suggest performing the sorption experiments associated with the evaluation of q_{max} at a certain value in the acidic pH range such as pH 3 or pH 4; the former is preferable for aerogel materials, in order to carry out experiments with total U(VI) concentration above the mmol range, which is needed to reach the plateau of the isothermal curves and accurately evaluate q_e values [38]. Indeed, the first three aerogels in terms of sorption capacity (Table 1) show maximum capacity in acidic solutions (pH 3-4), in which range UO_2^{2+} is the only species present [36–39].

At the molecular level, the optimum pH is associated in the case of inorganic oxides (e.g., Al_2O_3, TiO_2) with the point of zero charge (pzc) of the materials and the interaction of the negatively-charged surface with cationic U(VI) species at pH < 8 [10,11]. Below the pzc of the respective oxide, the adsorbent surface is positively charged due to surface protonation ($\equiv S–OH + H^+_{(aq)} \rightleftharpoons \equiv S–OH_2^+$; S: surface) and the sorption efficiency is low due to the electrostatic repulsion between the adsorbent surface and the cationic U(VI) species (e.g., UO_2^{2+}, UO_2OH^+, $(UO_2)_2(OH)_2^{2+}$). At pH values above the pzc, the surface hydroxyl groups are deprotonated ($\equiv S–OH + H_2O \rightleftharpoons \equiv S–O^- + H_3O^+$) and the surface attracts the positively-charged U(VI) resulting in enhanced sorption. However, above pH 6 and under ambient conditions the carbonate concentration in solution increases progressively resulting in the formation of very stable U(VI)-carbonato complexes, which stabilize U(VI) in solution and compete for U(VI) surface complexation [10,140,148].

Similarly, in the case of carbon-based aerogels the optimum pH lies in the weak acidic pH range (pH ~ 5) and is determined by the competing reactions, which are in the acidic pH range the protonation of surface active groups and in alkaline solutions the formation of U(VI) hydroxo- and carbonate complexes, which stabilize U(VI) in solution [10,140]. Under ambient conditions, the latter complexes are expected to govern the U(VI) in solution and have to be considered in associated species distribution diagrams. Adsorption on modified carbons has been observed via interaction of the metal species with sulfur (e.g., $–SO_3^-$) [67] or phosphorous (e.g., $–O–PO_3$) functionalities [66] at pH values 5-5.5.

2.2. Sorption Kinetics and Kinetic Modelling

In large-scale and industrial applications, fast and efficient sorption can reduce production costs and at the same time accelerate production efficiency. The adsorption kinetics describes the rate of adsorbate uptake on the adsorbent, which determines the adsorption equilibrium time. Therefore, investigations on sorption kinetics and kinetic data modelling are of fundamental importance. Most studies use the pseudo-first-order (eq. 1) and pseudo-second-order (eq. 2) adsorption kinetic models to analyze the experimental data.

$$q_t = q_e(1- e^{-k_1 t}) \tag{1}$$

$$q_t = \frac{k_2 {q_e}^2 t}{1 + k_2 q_e t} \tag{2}$$

Generally, due to the large number of active sites and functional groups on the surface of the aerogel materials, the U(VI) adsorption capacity increases rapidly with time. Generally, in an initial relatively fast step most of U(VI) is adsorbed and sorption continues until the systems reach equilibrium. The second step is characterized by a lower adsorption rate, which is attributed to the gradual occupation of surface active sites and the decrease of U(VI) concentration in solution [62]. With the exception of alumina-based aerogels [43], which need about 300 min to reach a steady-state, sorption on purely inorganic aerogels reaches maximum values within a few minutes [36,42,46]. Graphene-based aerogels reach equilibrium conditions mainly after ~50 min [61] and biomass-derived carbon aerogels need from 100 up to 1500 minutes to reach equilibrium [62], with the exception of polyurea-crosslinked calcium alginate (X-alginate) and calcium alginate aerogels that reach equilibrium within a few minutes [38]. Equally, fast adsorption was also observed for the corresponding polyurea aerogels [38].

Based on the linear correlation coefficients (R^2) and the calculated maximum adsorption capacity ($q_{\mathrm{max,\,cal}}$), which in the case of the pseudo-second-order kinetic model are close to unity and the experimental maximum adsorption capacity ($q_{\mathrm{max,exp}}$), respectively, sorption data are better described by the pseudo-second-order kinetic model, which could be in agreement with chemisorption [149]. Recent research supports the application of the non-linear form of the pseudo models for analyzing the adsorption kinetics otherwise erroneous conclusions may be derived [150].

2.3. Sorption Isotherms

The effect of the initial concentration on the sorption efficiency at constant temperature is of particular interest because it enables the fitting of the experimental data and evaluation of maximum adsorption values by applying simple empirical models (usually *Langmuir* and *Freundlich* adsorption isotherm models). Adsorption isotherms are essential for expressions of the theoretical maximum adsorption capacities and surface characteristics of the adsorbents, adsorption mechanism pathway optimization, and the productive design of the adsorption systems since they explain how model pollutants are interrelated with the materials of the adsorption process (adsorbents) [151]. Although in some cases these models are used to evaluate the adsorption mechanism (e.g., chemisorption) [71], this approach is very vague and should be used only as an indication.

According to Table 1, the maximum adsorption values (q_{max}) extend in a wide range between 13 g kg^{-1} and 2088 g kg^{-1}, with the highest values being among the highest ever reported for uranium adsorption; e.g., the recently reported values above 1800 g kg^{-1} are by far the highest found in the literature [36–39]. This is associated with the large surface area and hence the large number of active sites available for U(VI) binding on the aerogel materials. It has to be noted that extremely high q_{max} values have been reported for inorganic (hydroxyapatite) [36,37] as well as for biopolymer-based (X-alginate) [38] and carbon-based aerogels [39]. The only higher value than the above (q_{max}= 3550 g kg^{-1}) has been reported for graphene-based aerogels, which however act not as adsorbents, but as hosts of reagents that leach out of the aerogel matrix and cause precipitation of uranium from water [72].

2.4. Effect of Solution Composition and Competing Ions

In order to simulate real conditions, several investigations have focused on the effect of co-existing ions, such as K^+, Na^+, Ca^{2+}, Mg^{2+}, CO_3^{2-}, PO_4^{3-}, SO_4^{2-}, Cl^-, ClO_4^- and NO_3^-, on the U(VI) sorption by aerogels [34,36,43,44,58,62]. According to the related studies and the corresponding data that are summarized in Figure 4, conservative cations (e.g., K^+, Na^+) do not remarkably affect sorption efficiency, whereas in the presence of polyvalent metal ions (e.g., Ca^{2+}, Zn^{2+}, Al^{3+}) there is a significant decrease of the relative sorption efficiency [34,36,39,40,42–46,48,49,51,52,55,57–59,63,66,67]. This occurs because polyvalent metal cations can interact with surface moieties to form complexes, and therefore compete with U(VI) by occupying surface binding sites (Figure 5). The absence of any effect in the case of the conservative cations is a clear indication that U(VI) binding by the aerogels surface is based on specific interactions, which result in inner-sphere surface complexes, and not only because of pure electrostatic interactions associated with the formation of outer-sphere complexes [12–15].

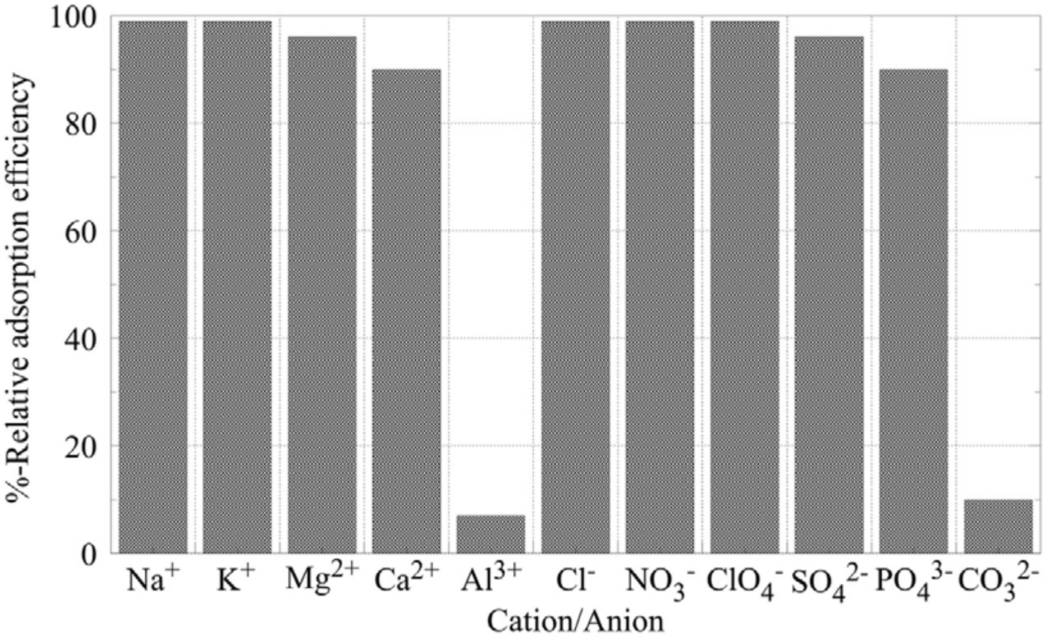

Figure 4. The effect of co-existing ions on the sorption of U(VI) by inorganic aerogels [42,44].

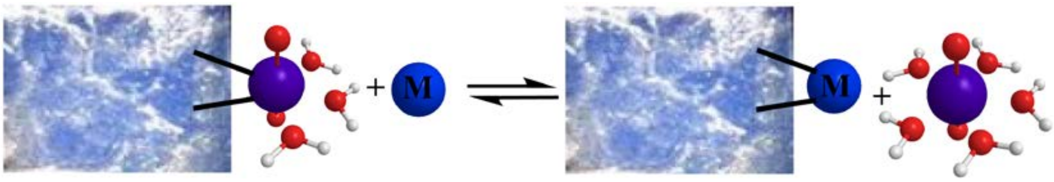

Figure 5. Schematic illustration of the competition reaction between U(VI) and competing cations (M^{z+}) regarding the sorption on aerogel surfaces. Charges are omitted for simplicity.

On the other hand, among the studied anions (Figure 4), only the presence of CO_3^{2-} and PO_4^{2-} in the solution seems to significantly affect reduced the relative U(VI) removal, because both CO_3^{2-} and PO_4^{2-} form very stable complexes with UO_2^{2+} (e.g., UO_2CO_3, $UO_2(CO_3)_2^{2-}$, $UO_2PO_4^-$ and UO_2HPO_4), which govern the U(VI) chemistry in the system [55,59,152]. The competitive interaction of U(VI) with carbonate cations to form the U(VI)-tricarbonato complex, which stabilizes U(VI) in aqueous solutions is schematically shown in Figure 6.

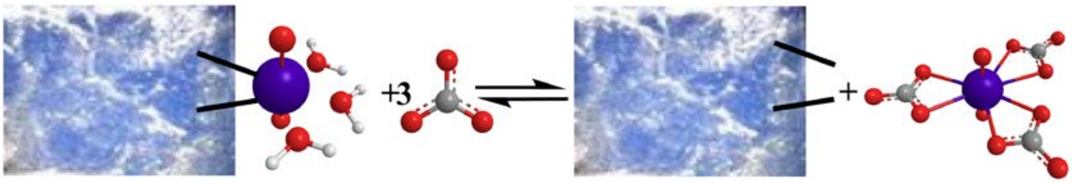

Figure 6. Schematic illustration of the stabilization of U(VI) in solution in the presence of carbonate ions by complex formation, which competes with surface complexation and sorption. Charges are omitted for simplicity.

Data obtained from these studies clearly show that the selectivity of the aerogel materials for uranium is limited and that the sorption capacity decreases remarkably in more complex aqueous laboratory solutions [36,41,43,64,67] and natural waters (e.g., seawater [38,41,47]). Hence, specific surface modifications (e.g., surface derivatization with salophen [153]) are needed to substantially increase selectivity towards U(VI) which will be only insignificantly affected by the presence of competing polyvalent metal ions, strong complexing anions (e.g., CO_3^{2-}) and acidic conditions ($pH < 3$).

2.5. Temperature Effect and Sorption Thermodynamics

Experiments related to the effect of temperature allow evaluation of sorption thermodynamics and calculation of the associated parameters (e.g., ΔH^o, ΔS^o and ΔG^o). The values of the thermodynamic parameters indicate whether sorption is an exothermic ($\Delta H^o < 0$) or an endothermic ($\Delta H^o > 0$), entropy-driven ($\Delta S^o > 0$) process. The Gibbs free energy change ΔG^o (kJ mol^{-1}) can be calculated from eq. (3) (van't Hoff equation) and it is connected with the enthalpy change (ΔH^o) and the entropy change (ΔS^o) through eq. (4), where R is the gas constant (8.314 J mol^{-1} K^{-1}), T is the absolute temperature (K) and K_e^0 is the thermodynamic equilibrium constant.

$$\Delta G^0 = -RT \ln K_e^0 \tag{3}$$

$$\Delta G^0 = \Delta H^0 - T\Delta S^0 \tag{4}$$

With the exception of one study only [61], all other studies up to now indicate that U(VI) sorption by aerogel materials is an endothermic, entropy-driven process and it is favoured with increasing temperature [38,39,49,51,52,54,55,58,61,62,64,65,67,68]. ΔH^o values can be as high as 141 kJ mol^{-1} and ΔS^o values can be as high as 500 J K^{-1} mol^{-1} (Table 2). The increase of entropy, which is the main driving force for U(VI) sorption by aerogels, is ascribed to the release of water molecules from the hydrated U(VI) ionic species and the charged surface moieties upon U(VI) surface complexation as schematically indicated in Figure 7.

Table 2. Literature values of ΔH^o and ΔS^o related to the U(VI) sorption by different aerogel materials.

Aerogel Material	ΔH^o (kJ mol^{-1})	ΔS^o (J K^{-1} mol^{-1})	Ref.
Reduced graphene oxide/ZIF-67 [a]	11.7	120	[39]
Bacterial cellulose@ZIF-8 carbon [b]	113.73	382.4	[49]
Nanocellulose	10.80	71.33	[51]
Chitosan/aluminum sludge composite	6.5	77	[52]
Iron-polyaniline-graphene composite	60.74	-	[54]
Chitosan/carboxylated carbon nanotube composite	21.96	157.3	[55]
Fungus hypha/graphene oxide	9.31	51.55	[58]
Graphene	-47.94	-73.03	[61]
Carbon/Fe_3O_4	141.4	500.2	[62]
Polydopamine- functionalized attapulgite/chitosan	5.45	50.24	[64]
p-Phthalaldehyde/3,5-diaminobenzoic acid-crosslinked chitosan	2.147	58.288	[65]
Sulfonated graphene	4.3	89.9	[67]
Graphene oxide/carbon nanotubes	8.146	91.43	[68]
Polyurea-crosslinked alginate (X-alginate)	>0	>0	[38]
Reduced graphene oxide/g-C_3N_4 quantum dots/ZIF-67 composite carbon [a]	>0	>0	[57]

[a] ZIF-67: Co-based zeolitic imidazole framework. b ZIF-8: Zn-based zeolitic imidazole framework.

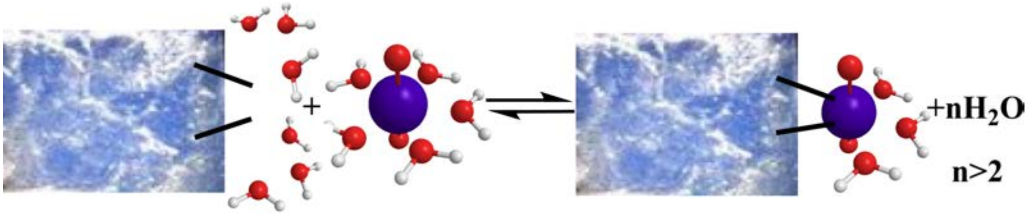

Figure 7. Schematic illustration of the water molecule release upon adsorption associated with the entropy increase leading to an entropy-driven adsorption process. Charges are omitted for simplicity.

2.6. Uranium Recovery and Material Recycling

Material recycling and uranium recovery are of particular interest from environmental and economic points of view. The former is related to the treatment of uranium-contaminated waters and uranium monitoring in the environment, and the latter is to the recovery of precious and industrial metals to cover increasing demands and compensate for the decline of natural resources. Regeneration studies have been carried out using EDTA solutions as extractants because EDTA has a strong ability to complex U(VI) without causing any damage to the adsorbent material [38]. Usually, five consecutive adsorption-desorption cycles are performed, and the recovery and regeneration efficiency are quantified to evaluate the process's applicability. The related studies have shown that the recovery and regeneration efficiency were satisfactory and the aerogel material remained almost intact [33,38,41,43,54,69]. The use of nitric acid solutions (0.5 M HNO_3) can result in the deterioration of the aerogel porous structure during the adsorption-desorption process and subsequently to the U(VI) recovery decline [64].

Despite the fact that carbonate solutions have been used as extractants for uranium recovery in other sorption studies [21] or often for the extraction of uranium from minerals/rocks, there are only a few studies [38] on the removal of U(VI) from aerogel materials making use of the high carbonate affinity for U(VI) to form very stable U(VI)-carbonato complexes [148], which is obvious from the solution composition and competing ions studies.

2.7. Effect of the Adsorbent Mass and Ionic Strength

Among the factors that affect U(VI) sorption by aerogels and have been investigated is the adsorbent dose. Generally, increasing the adsorbent dose results in an increase in the removal capacity but a gradual decline of the relative removal [42,62]. Increasing the amount of adsorbent is associated with an increase in the available surface area and the number of active sites and affects positively the sorption capacity, which reaches a maximum value and a plateau after a certain adsorbent amount. On the other hand, the relative sorption efficiency decreases because usually association of the adsorbent particles can lead to reduced relative adsorption efficiency.

Investigations on the effect of ionic strength on the adsorption could provide indications about the predominance of inner- or outer-sphere complex formation. Generally, when inner-sphere complexes are formed, which are characterized by a direct chemical bond between the surface functional groups of the adsorbent and the adsorbate, the sorption efficiency does not significantly depend on the ionic strength of the solution. On the other hand, if the adsorption is controlled mainly by outer-sphere complexes, which are based on pure electrostatic attraction and the ionic adsorbate retains its hydration sphere, the sorption efficiency is strongly affected by the ionic strength/salinity [152,154].

2.8. Spectroscopic Studies and Sorption Mechanism

Generally, the adsorption mechanism of U(VI) by aerogels is investigated by FTIR and XPS spectroscopy. Regarding FTIR, peak shifts and relative changes in peak intensities of surface-active groups (e.g., –COOH, –OH,) as well as the appearance of the characteristic uranyl (O=U=O) vibration in the spectrum after uranium sorption are employed to evaluate the adsorption mechanism. Interestingly, the peak shift of the uranyl moiety differs significantly from one type of aerogel to another and the values of the peak maximum vary between 895 cm^{-1} and 918 cm^{-1} [37,38,43,52,58,61,63,65]. On the other hand, changes in the relative area and binding energy of carbon and oxygen peaks associated with surface active moieties after U(VI) adsorption are used as a clear indication for surface complex formation [40,43,48,58,65]. In addition, the peaks at 383 eV in the high-resolution XPS spectra associated with U_{4f} are used to indicate complexation with surface groups [61]. EDS spectroscopy has also been applied after the adsorption tests to confirm the presence of uranium in the adsorbent material [38,54].

The information obtained from FTIR, XPS and EDS spectroscopic studies is very useful and associated data clearly indicate the surface-active groups which interact and form covalent bonds with the adsorbed uranium. However, a comprehensive description of the U(VI) binding on the aerogel surface at the molecular level is missing. In this context, EXAFS measurements along with theoretical calculations (e.g., DFT calculations [48]) would provide further insight into the adsorption mechanism. In addition to the spectroscopic methods, surface zeta potentials were used to point out the role of the surface charge with respect o U(VI) adsorption by aerogels materials [40].

Regarding the evaluation of the sorption mechanism, the spectroscopic measurements are of particular interest because the thermodynamic and kinetic data obtained from the sorption experiments are not specific for a single/defined reaction but correspond to an overall sorption reaction, which is the sum of the separate sorption reactions occurring at the aerogel surface. The number of the different sorption reactions depends on the surface homogeneity, the different active groups available on the surface and the U(VI) species which dominate in solution. The latter becomes significant for pH > 4 when hydrolysis and carbonate complexation are governing the solution chemistry of U(VI) [10,11,140].

2.9. Bulk Density of the Aerogel Material

Another property that has to be taken into consideration when practical applications to real conditions are targeted is the bulk density (ρ_β) of the aerogel material. Aerogels are famous for their extremely low bulk densities; however, in this particular case, this may not be an advantage. Indeed, our previous works [38,155] have shown that the calculation of the adsorption efficiency in g per litre ($q_{\max(V)}$) of the aerogel material (instead of g per kg ($q_{\max}$); Table 1) is very important and provides an estimation of the volume of the material needed for the uptake of a certain amount of uranium. For example, if we compare four aerogels from Table 1, i.e., polyurea-crosslinked alginate (X-alginate; $q_{\max}$ = 2023 g kg^{-1}, ρ_β = 150 g L^{-1}, $q_{\max(V)}$ = 303 g L^{-1}) [38], Al_2O_3/MgO ($q_{\max}$ = 1046.9 g kg^{-1}, ρ_β = 18.89 g L^{-1}, $q_{\max(V)}$ = 19.8 g L^{-1}) [40], calcium alginate ($q_{\max}$ = 388 g kg^{-1}, ρ_β = 68 g L^{-1}, $q_{\max(V)}$ = 26.4 g L^{-1}) [38] and aromatic polyurea derived from TIPM ($q_{\max}$ = 305 g kg^{-1}, ρ_β = 150 g L^{-1}, $q_{\max(V)}$ = 45.8 g L^{-1}) [38], it is obvious that X-alginate aerogels, with the highest density among the four aerogels, outperform by far the other three aerogels. That means that for the removal of 300 g of uranium, one would need 15.9 L of Al_2O_3/MgO, 11 L of calcium alginate, 6.6 L of polyurea, but only 1 L of X-alginate aerogels. A detailed presentation of $q_{\max(V)}$ for all aerogel materials for which bulk densities are reported has been published in reference [38].

3. Conclusions and Future Studies

The main conclusions that emerged from this review study can be summarized as follows:

In recent years, the number of studies regarding U(VI) sorption by aerogels has increased exponentially, because of the steadily increasing interest to produce efficient adsorbent materials for radionuclide removal and recovery from contaminated waters and industrial processes waters.

Generally, studies are dealing with the effect of different physicochemical parameters (e.g., pH, initial U(VI) concentration, ionic strength, temperature, contact time) on the adsorption efficiency. Among those parameters, pH plays a key role in affecting both U(VI) speciation and surface species dissociation and charge.

The isothermal data obtained from experiments related to the effect of metal ion concentration are best fitted with the Langmuir adsorption isotherm model resulting in supreme sorption capacity values (in some cases even above 2000 g of uranium per kg of aerogel). The experimental kinetic data indicate fast sorption kinetics (equilibrium conditions are reached between minutes to a few hours) and are best fitted by the pseudo-second-order kinetic model. It has to be mentioned that both the Langmuir isotherm and the pseudo-second-order kinetic models are indicative of chemisorption. The latter is indicated also by the effect of the adsorbent dose and the effect of the ionic strength. In addition, the associated thermodynamic data, which in most cases show an endothermic, entropy-driven sorption mechanism, are indicating the formation of inner-sphere surface complexes.

The presence of multivalent metal cations (e.g., Ca^{2+}, Al^{3+}) and complexing species (e.g., CO_3^{2-}, PO_4^{3-}) strongly affect the sorption efficiency of the adsorbents towards uranium, because of competitive sorption and formation of stable solution complexes, respectively. Moreover, the data show that the aerogel materials show excellent performance regarding their reuse even after several adsorption-desorption cycles and uranium recovery.

Spectroscopic studies based mainly on FTIR and XPS measurements clearly indicate the formation of inner-sphere complexes between U(VI) and the active groups on the aerogel surfaces.

Based on this review future studies should focus on the preparation of aerogel materials with specific surface groups possessing high affinity and selectivity towards uranium and other precious and industrial metals/metalloids. The selective aerogel materials should be tested not only in lab and "real" solutions but also at pilot and industrial scale applications. Moreover, data obtained from EXAFS (Extended X-ray absorption fine structure spectroscopy) and TRLFS (Time-resolved laser fluorescence spectroscopy) studies would allow a better understanding of the interaction between U(VI) species and the aerogel surface and describe the mechanism at the molecular level.

Author Contributions: Conceptualization, M.A., P.P. and I.P.; methodology, P.P. and I.P.; investigation, E.G., G.R. and P.P.; resources, D.A.G., M.A., E.G., G.R. and P.P.; writing—original draft preparation, E.G., G.R., P.P. and I.P.; writing—review and editing, I.A., M.A., D.A.G., E.G., G.R. and PP.; visualization, D.A.G., M.A., I.P., and PP; supervision, I.A., D.A.G., M.A., I.P. and P.P.; All authors have read and agreed to the published version of the manuscript.

Funding: This publication is based upon work from COST Action "Advanced Engineering of aeroGels for Environment and Life Sciences" (AERoGELS, ref. CA18125), supported by COST (European Co-operation in Science and Technology). The Special Account of Research Grants of the National and Kapodistrian University of Athens is also acknowledged.

Data Availability Statement: Not applicable

Conflicts of Interest: The authors declare no conflict of interest

References

1. Veglio', F.; Beolchini, F. Removal of Metals by Biosorption: A Review. *Hydrometallurgy* **1997**, *44*, 301–316, doi:10.1016/S0304-386X(96)00059-X.
2. Gazso, G.L. The Key Microbial Processes in the Removal of Toxic Metals and Radionuclides from the Environment. *Central European Journal of Occupational and Environmental Medicine Hungary* **2001**.
3. Ishikawa, S.-I.; Suyama, K.; Arihara, K.; Itoh, M. Selective Recovery of Uranium and Thorium Ions from Dilute Aqueous Solutions by Animal Biopolymers. *Biol Trace Elem Res* **2002**, *86*, 227–236, doi:10.1385/BTER:86:3:227.
4. Srinivasa Gowd, S.; Govil, P.K. Distribution of Heavy Metals in Surface Water of Ranipet Industrial Area in Tamil Nadu, India. *Environ Monit Assess* **2008**, *136*, 197–207, doi:10.1007/s10661-007-9675-5.
5. D. Brugge; J. L. deLemos; B. Oldmixon Exposure Pathways and Health Effects Associated with Chemical and Radiological Toxicity of Natural Uranium: A Review. *Reviews on Environmental Health* **2005**, *20*, 177–194, doi:10.1515/REVEH.2005.20.3.177.
6. Anastopoulos, I.; Massas, I.; Ehaliotis, C. Use of Residues and By-Products of the Olive-Oil Production Chain for the Removal of Pollutants from Environmental Media: A Review of Batch Biosorption Approaches. *Journal of Environmental Science and Health, Part A* **2015**, *50*, 677–718, doi:10.1080/10934529.2015.1011964.
7. Raffa, C.M.; Chiampo, F.; Shanthakumar, S. Remediation of Metal/Metalloid-Polluted Soils: A Short Review. *Applied Sciences* **2021**, *11*, 4134, doi:10.3390/app11094134.
8. Bleise, A.; Danesi, P.R.; Burkart, W. Properties, Use and Health Effects of Depleted Uranium (DU): A General Overview. *Journal of Environmental Radioactivity* **2003**, *64*, 93–112, doi:10.1016/S0265-931X(02)00041-3.
9. Markich, S.J. Uranium Speciation and Bioavailability in Aquatic Systems: An Overview. *The Scientific World Journal* **2002**, *2*, 707–729, doi:10.1100/tsw.2002.130.
10. Mühr-Ebert, E.L.; Wagner, F.; Walther, C. Speciation of Uranium: Compilation of a Thermodynamic Database and Its Experimental Evaluation Using Different Analytical Techniques. *Applied Geochemistry* **2019**, *100*, 213–222, doi:10.1016/j.apgeochem.2018.10.006.
11. Fanghänel, T.; Neck, V. Aquatic Chemistry and Solubility Phenomena of Actinide Oxides/Hydroxides. *Pure and Applied Chemistry* **2002**, *74*, 1895–1907, doi:10.1351/pac200274101895.
12. Philippou, K.; Savva, I.; Pashalidis, I. Uranium(VI) Binding by Pine Needles Prior and after Chemical Modification. *J Radioanal Nucl Chem* **2018**, *318*, 2205–2211, doi:10.1007/s10967-018-6145-1.
13. Liatsou, I.; Michail, G.; Demetriou, M.; Pashalidis, I. Uranium Binding by Biochar Fibres Derived from Luffa Cylindrica after Controlled Surface Oxidation. *J Radioanal Nucl Chem* **2017**, *311*, 871–875, doi:10.1007/s10967-016-5063-3.
14. Hadjittofi, L.; Pashalidis, I. Uranium Sorption from Aqueous Solutions by Activated Biochar Fibres Investigated by FTIR Spectroscopy and Batch Experiments. *J Radioanal Nucl Chem* **2015**, *304*, 897–904, doi:10.1007/s10967-014-3868-5.
15. Stasi, C.; Georgiou, E.; Ioannidis, I.; Pashalidis, I. Uranium Removal from Laboratory and Environmental Waters by Oxidised Biochar Prepared from Palm Tree Fibres. *J Radioanal Nucl Chem* **2022**, *331*, 375–381, doi:10.1007/s10967-021-08076-1.
16. Bhalara, P.D.; Punetha, D.; Balasubramanian, K. A Review of Potential Remediation Techniques for Uranium(VI) Ion Retrieval from Contaminated Aqueous Environment. *Journal of Environmental Chemical Engineering* **2014**, *2*, 1621–1634, doi:10.1016/j.jece.2014.06.007.
17. Gupta, R.; Ahuja, P.; Khan, S.; Saxena, R.K.; Mohapatra, H. Microbial Biosorbents: Meeting Challenges of Heavy Metal Pollution in Aqueous Solutions. *Current Science* **2000**, *78*, 967–973.
18. Giannakoudakis, D.A.; Anastopoulos, I.; Barczak, M.; Antoniou, E.; Terpiłowski, K.; Mohammadi, E.; Shams, M.; Coy, E.; Bakandritsos, A.; Katsoyiannis, I.A.; Colmenares, J.C.; Pashalidis, I. Enhanced Uranium Removal from Acidic Wastewater by Phosphonate-Functionalized Ordered Mesoporous Silica: Surface Chemistry Matters the Most. *Journal of Hazardous Materials* **2021**, *413*, 125279, doi:10.1016/j.jhazmat.2021.125279.
19. Ioannou, K.; Hadjiyiannis, P.; Liatsou, I.; Pashalidis, I. U(VI) Adsorption by Biochar Fiber–MnO_2 Composites. *J Radioanal Nucl Chem* **2019**, *320*, 425–432, doi:10.1007/s10967-019-06479-9.
20. Christou, C.; Philippou, K.; Krasia-Christoforou, T.; Pashalidis, I. Uranium Adsorption by Polyvinylpyrrolidone/Chitosan Blended Nanofibers. *Carbohydrate Polymers* **2019**, *219*, 298–305, doi:10.1016/j.carbpol.2019.05.041.
21. Philippou, K.; Anastopoulos, I.; Dosche, C.; Pashalidis, I. Synthesis and Characterization of a Novel Fe_3O_4-Loaded Oxidized Biochar from Pine Needles and Its Application for Uranium Removal. Kinetic, Thermodynamic, and Mechanistic Analysis. *Journal of Environmental Management* **2019**, *252*, 109677, doi:10.1016/j.jenvman.2019.109677.
22. Philippou, K.; Christou, C.N.; Socoliuc, V.; Vekas, L.; Tanasă, E.; Miclau, M.; Pashalidis, I.; Krasia-Christoforou, T. Superparamagnetic Polyvinylpyrrolidone/Chitosan/Fe_3O_4 Electrospun Nanofibers as Effective U(VI) Adsorbents. *Journal of Applied Polymer Science* **2021**, *138*, 50212, doi:10.1002/app.50212.
23. Anastopoulos, I.; Milojković, J.V.; Tsigkou, K.; Zafiri, C.; Lopičić, Z.R.; Kornaros, M.; Pashalidis, I. A Nappies Management By-Product for the Treatment of Uranium-Contaminated Waters. *Journal of Hazardous Materials* **2021**, *404*, 124147, doi:10.1016/j.jhazmat.2020.124147.
24. Ilia, R.; Liatsou, I.; Savva, I.; Vasile, E.; Vekas, L.; Marinica, O.; Mpekris, F.; Pashalidis, I.; Krasia-Christoforou, T. Magnetoresponsive Polymer Networks as Adsorbents for the Removal of U(VI) Ions from Aqueous Media. *European Polymer Journal* **2017**, *97*, 138–146, doi:10.1016/j.eurpolymj.2017.10.005.

25. Arkas, M.; Anastopoulos, I.; Giannakoudakis, D.A.; Pashalidis, I.; Katsika, T.; Nikoli, E.; Panagiotopoulos, R.; Fotopoulou, A.; Vardavoulias, M.; Douloudi, M. Catalytic Neutralization of Water Pollutants Mediated by Dendritic Polymers. *Nanomaterials* **2022**, *12*, 445, doi:10.3390/nano12030445.
26. Panagiotou, N.; Liatsou, I.; Pournara, A.; Angeli, G.K.; Giappa, R.M.; Tylianakis, E.; Manos, M.J.; Froudakis, G.E.; Trikalitis, P.N.; Pashalidis, I.; Tasiopoulos, A.J. Water-Stable 2-D Zr MOFs with Exceptional UO$_2^{2+}$ Sorption Capability. *J. Mater. Chem. A* **2020**, *8*, 1849–1857, doi:10.1039/C9TA10701K.
27. Liu, H.; Fu, T.; Mao, Y. Metal–Organic Framework-Based Materials for Adsorption and Detection of Uranium(VI) from Aqueous Solution. *ACS Omega* **2022**, *7*, 14430–14456, doi:10.1021/acsomega.2c00597.
28. Koppula, S.; Manabolu Surya, S.; Katari, N.K.; Dhami, P.S.; Sivasankaran Nair, R.K. Mesoporous MOF Composite for Efficient Removal of Uranium, Methyl Orange, Methylene Blue, and Congo Red Dyes from Aqueous Solutions. *Applied Organometallic Chemistry* **2022**, *36*, e6554, doi:10.1002/aoc.6554.
29. Guo, H.; Mei, P.; Xiao, J.; Huang, X.; Ishag, A.; Sun, Y. Carbon Materials for Extraction of Uranium from Seawater. *Chemosphere* **2021**, *278*, 130411, doi:10.1016/j.chemosphere.2021.130411.
30. Guo, D.; Song, X.; Zhang, L.; Chen, W.; Chu, D.; Tan, L. Recovery of Uranium (VI) from Aqueous Solutions by the Polyethyleneimine-Functionalized Reduced Graphene Oxide/Molybdenum Disulfide Composition Aerogels. *Journal of the Taiwan Institute of Chemical Engineers* **2020**, *106*, 198–205, doi:10.1016/j.jtice.2019.09.029.
31. Huang, Z.; Li, Z.; Zheng, L.; Zhou, L.; Chai, Z.; Wang, X.; Shi, W. Interaction Mechanism of Uranium(VI) with Three-Dimensional Graphene Oxide-Chitosan Composite: Insights from Batch Experiments, IR, XPS, and EXAFS Spectroscopy. *Chemical Engineering Journal* **2017**, *328*, 1066–1074, doi:10.1016/j.cej.2017.07.067.
32. Coleman, S.J.; Coronado, P.R.; Maxwell, R.S.; Reynolds, J.G. Granulated Activated Carbon Modified with Hydrophobic Silica Aerogel-Potential Composite Materials for the Removal of Uranium from Aqueous Solutions. *Environ. Sci. Technol.* **2003**, *37*, 2286–2290, doi:10.1021/es020929e.
33. Jiang, X.; Wang, H.; Hu, E.; Lei, Z.; Fan, B.; Wang, Q. Efficient Adsorption of Uranium from Aqueous Solutions by Microalgae Based Aerogel. *Microporous and Mesoporous Materials* **2020**, *305*, 110383, doi:10.1016/j.micromeso.2020.110383.
34. Yin, J.; Yang, S.; He, W.; Zhao, T.; Li, C.; Hua, D. Biogene-Derived Aerogels for Simultaneously Selective Adsorption of Uranium(VI) and Strontium(II) by Co-Imprinting Method. *Separation and Purification Technology* **2021**, *271*, 118849, doi:10.1016/j.seppur.2021.118849.
35. Yu, J.; Wang, J.; Jiang, Y. Removal of Uranium from Aqueous Solution by Alginate Beads. *Nuclear Engineering and Technology* **2017**, *49*, 534–540, doi:10.1016/j.net.2016.09.004.
36. Xiong, T.; Li, Q.; Liao, J.; Zhang, Y.; Zhu, W. Highly Enhanced Adsorption Performance to Uranium(VI) by Facile Synthesized Hydroxyapatite Aerogel. *Journal of Hazardous Materials* **2022**, *423*, 127184, doi:10.1016/j.jhazmat.2021.127184.
37. Xiong, T.; Li, Q.; Liao, J.; Zhang, Y.; Zhu, W. Design of Hydroxyapatite Aerogel with Excellent Adsorption Performance to Uranium. *Journal of Environmental Chemical Engineering* **2021**, *9*, 106364, doi:10.1016/j.jece.2021.106364.
38. Georgiou, E.; Raptopoulos, G.; Papastergiou, M.; Paraskevopoulou, P.; Pashalidis, I. Extremely Efficient Uranium Removal from Aqueous Environments with Polyurea-Cross-Linked Alginate Aerogel Beads. *ACS Appl. Polym. Mater.* **2022**, doi:10.1021/acsapm.1c01400.
39. Zhao, M.; Tesfay Reda, A.; Zhang, D. Reduced Graphene Oxide/ZIF-67 Aerogel Composite Material for Uranium Adsorption in Aqueous Solutions. *ACS Omega* **2020**, *5*, 8012–8022, doi:10.1021/acsomega.0c00089.
40. Lei, Y.; Li, K.; Liao, J.; Zhang, Y.; Zhang, L.; Zhu, W. Design of 3D Alumina-Doped Magnesium Oxide Aerogels with a High Efficiency Removal of Uranium(VI) from Wastewater. *Inorg. Chem. Front.* **2021**, *8*, 2561–2574, doi:10.1039/D1QI00259G.
41. Chen, M.; Liu, T.; Zhang, X.; Zhang, R.; Tang, S.; Yuan, Y.; Xie, Z.; Liu, Y.; Wang, H.; Fedorovich, K.V.; Wang, N. Photoinduced Enhancement of Uranium Extraction from Seawater by MOF/Black Phosphorus Quantum Dots Heterojunction Anchored on Cellulose Nanofiber Aerogel. *Advanced Functional Materials* **2021**, *31*, 2100106, doi:10.1002/adfm.202100106.
42. Liao, J.; Liu, P.; Xie, Y.; Zhang, Y. Metal Oxide Aerogels: Preparation and Application for the Uranium Removal from Aqueous Solution. *Science of The Total Environment* **2021**, *768*, 144212, doi:10.1016/j.scitotenv.2020.144212.
43. Ding, L.; Liao, J.; Zhang, Y. Adsorption Performance and Mechanism of Al$_2$O$_3$ Aerogels towards Aqueous U(VI) Using Template Synthesis Technology. *Colloids and Surfaces A: Physicochemical and Engineering Aspects* **2021**, *612*, 125980, doi:10.1016/j.colsurfa.2020.125980.
44. Liao, J.; Zhang, Y.; Zhang, L. Improved Catalytic Activity on the Thermal Decomposition of Ammonium Perchlorate and Efficient Adsorption of Uranium Using a Novel Ultra-Low Density Al$_2$O$_3$-Based Aerogels. *Journal of Hazardous Materials* **2020**, *387*, 122015, doi:10.1016/j.jhazmat.2020.122015.
45. Li, N.; Yang, L.; Wang, D.; Tang, C.; Deng, W.; Wang, Z. High-Capacity Amidoxime-Functionalized β-Cyclodextrin/Graphene Aerogel for Selective Uranium Capture. *Environ. Sci. Technol.* **2021**, *55*, 9181–9188, doi:10.1021/acs.est.0c08743.
46. Liao, J.; Zhang, Y.; He, X.; Zhang, L.; He, Z. The Synthesis of a Novel Titanium Oxide Aerogel with Highly Enhanced Removal of Uranium and Evaluation of the Adsorption Mechanism. *Dalton Trans.* **2021**, *50*, 3616–3628, doi:10.1039/D0DT04320F.
47. Dang, Z.; Jia, M.; Liao, J.; Zhang, Y.; Zhu, W. Fabrication of the Al$_2$O$_3$ Aerogels by in Situ Water Formation Method for the Highly Efficient Removal of Uranium(VI). *Microporous and Mesoporous Materials* **2021**, *316*, 110952, doi:10.1016/j.micromeso.2021.110952.
48. Wang, Y.; Hu, X.; Liu, Y.; Li, Y.; Lan, T.; Wang, C.; Liu, Y.; Yuan, D.; Cao, X.; He, H.; Zhou, L.; Liu, Z.; Chew, J.W. Assembly of Three-Dimensional Ultralight Poly(Amidoxime)/Graphene Oxide Nanoribbons Aerogel for Efficient Removal of Uranium(VI) from Water Samples. *Science of The Total Environment* **2021**, *765*, 142686, doi:10.1016/j.scitotenv.2020.142686.

49. Zhou, Q.; Chen, J.; Jin, B.; Chu, S.; Peng, R. Modification of ZIF-8 on Bacterial Cellulose for an Efficient Selective Capture of U(VI). *Cellulose* **2021**, *28*, 5241–5256, doi:10.1007/s10570-021-03820-y.
50. Hu, Y.; Pan, C.; Liu, S.; Wang, X.; Zheng, X.; Hu, F.; Xu, L.; Xu, G.; Jian, Y.; Peng, X. Ultra-Fast Adsorption of Radioactive-U(VI) and Cs(I) with High Adsorption Capacity towards CAA@MgAlFe Spongy-like Aerogel: Mechanism and Application Feasibility Study. *Journal of Nuclear Materials* **2022**, *559*, 153463, doi:10.1016/j.jnucmat.2021.153463.
51. Wang, Y.; Li, Y.; Zhang, Y.; Zhang, Z.; Li, Y.; Li, W. Nanocellulose Aerogel for Highly Efficient Adsorption of Uranium (VI) from Aqueous Solution. *Carbohydrate Polymers* **2021**, *267*, 118233, doi:10.1016/j.carbpol.2021.118233.
52. Liu, W.; Zhang, L.; Chen, F.; Wang, H.; Wang, Q.; Liang, K. Efficiency and Mechanism of Adsorption of Low-Concentration Uranium from Water by a New Chitosan/Aluminum Sludge Composite Aerogel. *Dalton Trans.* **2020**, *49*, 3209–3221, doi:10.1039/C9DT04670D.
53. Li, Y.; He, H.; Liu, Z.; Lai, Z.; Wang, Y. A Facile Method for Preparing Three-Dimensional Graphene Nanoribbons Aerogel for Uranium(VI) and Thorium(IV) Adsorption. *J Radioanal Nucl Chem* **2021**, *328*, 289–298, doi:10.1007/s10967-021-07619-w.
54. Chen, L.; Feng, S.; Zhao, D.; Chen, S.; Li, F.; Chen, C. Efficient Sorption and Reduction of U(VI) on Zero-Valent Iron-Polyaniline-Graphene Aerogel Ternary Composite. *Journal of Colloid and Interface Science* **2017**, *490*, 197–206, doi:10.1016/j.jcis.2016.11.050.
55. Tang, X.; Zhou, L.; Le, Z.; Wang, Y.; Liu, Z.; Huang, G.; Adesina, A.A. Preparation of Porous Chitosan/Carboxylated Carbon Nanotube Composite Aerogels for the Efficient Removal of Uranium(VI) from Aqueous Solution. *International Journal of Biological Macromolecules* **2020**, *160*, 1000–1008, doi:10.1016/j.ijbiomac.2020.05.179.
56. Wu, F.; Liu, D.; Li, G.; Li, L.; Yan, L.; Hong, G.; Zhang, X. Bayberry Tannin Directed Assembly of a Bifunctional Graphene Aerogel for Simultaneous Solar Steam Generation and Marine Uranium Extraction. *Nanoscale* **2021**, *13*, 5419–5428, doi:10.1039/D0NR08956G.
57. Zhou, Q.; Jin, B.; Zhao, P.; Chu, S.; Peng, R. RGO/CNQDs/ZIF-67 Composite Aerogel for Efficient Extraction of Uranium in Wastewater. *Chemical Engineering Journal* **2021**, *419*, 129622, doi:10.1016/j.cej.2021.129622.
58. Li, Y.; Li, L.; Chen, T.; Duan, T.; Yao, W.; Zheng, K.; Dai, L.; Zhu, W. Bioassembly of Fungal Hypha/Graphene Oxide Aerogel as High Performance Adsorbents for U(VI) Removal. *Chemical Engineering Journal* **2018**, *347*, 407–414, doi:10.1016/j.cej.2018.04.140.
59. Li, J.; Wang, J.; Wang, W.; Zhang, X. Symbiotic Aerogel Fibers Made via In-Situ Gelation of Aramid Nanofibers with Polyamidoxime for Uranium Extraction. *Molecules* **2019**, *24*, 1821, doi:10.3390/molecules24091821.
60. Liao, J.; Li, K.; Zhang, Y.; Zhang, L. Facile Synthesis of a Novel Ultra-Low Density Praseodymium Oxide Aerogel for Catalyst and Adsorbent. *Materials Letters* **2019**, *254*, 364–366, doi:10.1016/j.matlet.2019.07.108.
61. Zhao, D.; Wang, Y.; Zhao, S.; Wakeel, M.; Wang, Z.; Shaikh, R.S.; Hayat, T.; Chen, C. A Simple Method for Preparing Ultra-Light Graphene Aerogel for Rapid Removal of U(VI) from Aqueous Solution. *Environmental Pollution* **2019**, *251*, 547–554, doi:10.1016/j.envpol.2019.05.011.
62. Yin, N.; Ai, Y.; Xu, Y.; Ouyang, Y.; Yang, P. Preparation of Magnetic Biomass-Carbon Aerogel and Its Application for Adsorption of Uranium(VI). *J Radioanal Nucl Chem* **2020**, *326*, 1307–1321, doi:10.1007/s10967-020-07392-2.
63. He, Y.-R.; Li, X.-L.; Li, X.-L.; Tan, Z.-Y.; Zhang, D.; Chen, H.-B. Aerogel Based on Melamine-Formaldehyde and Alginate: Simply Removing of Uranium from Aqueous Solutions. *Journal of Molecular Liquids* **2019**, *289*, 111154, doi:10.1016/j.molliq.2019.111154.
64. Liao, Y.; Wang, M.; Chen, D. Production of Three-Dimensional Porous Polydopamine-Functionalized Attapulgite/Chitosan Aerogel for Uranium(VI) Adsorption. *J Radioanal Nucl Chem* **2018**, *316*, 635–647, doi:10.1007/s10967-018-5816-2.
65. Yang, L.; Huang, C.; Luo, X.; Zhang, L.; Ye, Y.; Jun, H.; Wang, Y. Chitosan-Based Aerogel with Anti-Swelling for U(VI) Adsorption from Aqueous Solution. *Colloids and Surfaces A: Physicochemical and Engineering Aspects* **2021**, *630*, 127527, doi:10.1016/j.colsurfa.2021.127527.
66. Zhang, Z.; Dong, Z.; Wang, X.; Dai, Y.; Cao, X.; Wang, Y.; Hua, R.; Feng, H.; Chen, J.; Liu, Y.; Hu, B.; Wang, X. Synthesis of Ultralight Phosphorylated Carbon Aerogel for Efficient Removal of U(VI): Batch and Fixed-Bed Column Studies. *Chemical Engineering Journal* **2019**, *370*, 1376–1387, doi:10.1016/j.cej.2019.04.012.
67. Zhang, Z.; Huang, J.; Dong, Z.; Luo, B.; Liu, Y.; Dai, Y.; Cao, X.; Wang, Y.; Hua, R.; Liu, Y. Ultralight Sulfonated Graphene Aerogel for Efficient Adsorption of Uranium from Aqueous Solutions. *J Radioanal Nucl Chem* **2019**, *321*, 1045–1055, doi:10.1007/s10967-019-06641-3.
68. Gu, Z.; Wang, Y.; Tang, J.; Yang, J.; Liao, J.; Yang, Y.; Liu, N. The Removal of Uranium(VI) from Aqueous Solution by Graphene Oxide–Carbon Nanotubes Hybrid Aerogels. *J Radioanal Nucl Chem* **2015**, *303*, 1835–1842, doi:10.1007/s10967-014-3795-5.
69. Dubey, S.P.; Dwivedi, A.D.; Kim, I.-C.; Sillanpaa, M.; Kwon, Y.-N.; Lee, C. Synthesis of Graphene–Carbon Sphere Hybrid Aerogel with Silver Nanoparticles and Its Catalytic and Adsorption Applications. *Chemical Engineering Journal* **2014**, *244*, 160–167, doi:10.1016/j.cej.2014.01.042.
70. Riley, B.J.; Chun, J.; Um, W.; Lepry, W.C.; Matyas, J.; Olszta, M.J.; Li, X.; Polychronopoulou, K.; Kanatzidis, M.G. Chalcogen-Based Aerogels As Sorbents for Radionuclide Remediation. *Environ. Sci. Technol.* **2013**, *47*, 7540–7547, doi:10.1021/es400595z.
71. Wang, Z.; Liu, H.; Lei, Z.; Huang, L.; Wu, T.; Liu, S.; Ye, G.; Lu, Y.; Wang, X. Graphene Aerogel for Photocatalysis-Assist Uranium Elimination under Visible Light and Air Atmosphere. *Chemical Engineering Journal* **2020**, *402*, 126256, doi:10.1016/j.cej.2020.126256.
72. Wang, Z.; Hu, H.; Huang, L.; Lin, F.; Liu, S.; Wu, T.; Alharbi, N.S.; Rabah, S.O.; Lu, Y.; Wang, X. Graphene Aerogel Capsulated Precipitants for High Efficiency and Rapid Elimination of Uranium from Water. *Chemical Engineering Journal* **2020**, *396*, 125272, doi:10.1016/j.cej.2020.125272.
73. Leventis, N.; Sadekar, A.; Chandrasekaran, N.; Sotiriou-Leventis, C. Click Synthesis of Monolithic Silicon Carbide Aerogels from Polyacrylonitrile-Coated 3D Silica Networks. *Chem. Mater.* **2010**, *22*, 2790–2803, doi:10.1021/cm903662a.

74. Vareda, J.P.; Lamy-Mendes, A.; Durães, L. A Reconsideration on the Definition of the Term Aerogel Based on Current Drying Trends. *Microporous and Mesoporous Materials* **2018**, *258*, 211–216, doi:10.1016/j.micromeso.2017.09.016.
75. Aegerter, M.A.; Leventis, N.; Koebel, M.M. *Aerogels Handbook*; Springer Science & Business Media, 2011; ISBN 978-1-4419-7589-8.
76. Kistler, S.S. Coherent Expanded Aerogels and Jellies. *Nature* **1931**, *127*, 741, doi:10.1038/127741a0.
77. Kistler, S.S. The Relation between Heat Conductivity and Structure in Silica Aerogel. *J. Phys. Chem.* **1934**, *39*, 79–86, doi:10.1021/j150361a006.
78. Kistler, S.S. Coherent Expanded-Aerogels. *J. Phys. Chem.* **1931**, *36*, 52–64, doi:10.1021/j150331a003.
79. Kistler, S.S.; Swann, S.; Appel, E.G. Aerogel Catalysts - Thoria: Preparation of Catalyst and Conversions of Organic Acids to Ketones. *Ind. Eng. Chem.* **1934**, *26*, 388–391, doi:10.1021/ie50292a007.
80. Kistler, S.S. Method of Making Aerogels, US2249767A 1941.
81. Peri, J.B. Infrared Study of OH and NH_2 Groups on the Surface of a Dry Silica Aerogel. *J. Phys. Chem.* **1966**, *70*, 2937–2945, doi:10.1021/j100881a037.
82. Arenillas, A.; Menéndez, J.A.; Reichenauer, G.; Celzard, A.; Fierro, V.; Hodar, F.J.M.; Bailón-Garcia, E.; Job, N. *Organic and Carbon Gels: From Laboratory Synthesis to Applications*; Springer, 2019; ISBN 978-3-030-13897-4.
83. Ratke, L.; Gurikov, P. *The Chemistry and Physics of Aerogels: Synthesis, Processing, and Properties*; Cambridge University Press, 2021; ISBN 978-1-108-80540-7.
84. Du, A.; Zhou, B.; Zhang, Z.; Shen, J. A Special Material or a New State of Matter: A Review and Reconsideration of the Aerogel. *Materials* **2013**, *6*, 941–968, doi:10.3390/ma6030941.
85. Stepanian, C. Highly Flexible Aerogel Insulated Textile-like Blankets, US20070154698A1 2007.
86. Tafreshi, O.A.; Mosanenzadeh, S.G.; Karamikamkar, S.; Saadatnia, Z.; Park, C.B.; Naguib, H.E. A Review on Multifunctional Aerogel Fibers: Processing, Fabrication, Functionalization, and Applications. *Materials Today Chemistry* **2022**, *23*, 100736, doi:10.1016/j.mtchem.2021.100736.
87. Cashman, J.L.; Nguyen, B.N.; Dosa, B.; Meador, M.A.B. Flexible Polyimide Aerogels Derived from the Use of a Neopentyl Spacer in the Backbone. *ACS Appl. Polym. Mater.* **2020**, *2*, 2179–2189, doi:10.1021/acsapm.0c00153.
88. Meador, M.A.B.; Alemán, C.R.; Hanson, K.; Ramirez, N.; Vivod, S.L.; Wilmoth, N.; McCorkle, L. Polyimide Aerogels with Amide Cross-Links: A Low Cost Alternative for Mechanically Strong Polymer Aerogels. *ACS Applied Materials & Interfaces* **2015**, *7*, 1240–1249, doi:10.1021/am507268c.
89. Ganesan, K.; Budtova, T.; Ratke, L.; Gurikov, P.; Baudron, V.; Preibisch, I.; Niemeyer, P.; Smirnova, I.; Milow, B. Review on the Production of Polysaccharide Aerogel Particles. *Materials* **2018**, *11*, 2144, doi:10.3390/ma11112144.
90. Paraskevopoulou, P.; Chriti, D.; Raptopoulos, G.; Anyfantis, G.C. Synthetic Polymer Aerogels in Particulate Form. *Materials* **2019**, *12*, 1543, doi:10.3390/ma12091543.
91. Chriti, D.; Raptopoulos, G.; Papastergiou, M.; Paraskevopoulou, P. Millimeter-Size Spherical Polyurea Aerogel Beads with Narrow Size Distribution. *Gels* **2018**, *4*, 66, doi:10.3390/gels4030066.
92. Leventis, N.; Trifu, R.; Begag, R.; Gould, G.L.; Zafiropoulos, N.A.; Miller, H.R. Aqueous Polyimide Processes, US20220185970A1 2022.
93. Bang, A.; Buback, C.; Sotiriou-Leventis, C.; Leventis, N. Flexible Aerogels from Hyperbranched Polyurethanes: Probing the Role of Molecular Rigidity with Poly(Urethane Acrylates) Versus Poly(Urethane Norbornenes). *Chem. Mater.* **2014**, *26*, 6979–6993, doi:10.1021/cm5031443.
94. Paraskevopoulou, P.; Raptopoulos, G.; Len, A.; Dudás, Z.; Fábián, I.; Kalmár, J. Fundamental Skeletal Nanostructure of Nanoporous Polymer-Cross-Linked Alginate Aerogels and Its Relevance To Environmental Remediation. *ACS Appl. Nano Mater.* **2021**, *4*, 10575–10583, doi:10.1021/acsanm.1c02072.
95. Kanellou, A.; Anyfantis, G.C.; Chriti, D.; Raptopoulos, G.; Pitsikalis, M.; Paraskevopoulou, P. Poly(Urethane-Norbornene) Aerogels via Ring Opening Metathesis Polymerization of Dendritic Urethane-Norbornene Monomers: Structure-Property Relationships as a Function of an Aliphatic Versus an Aromatic Core and the Number of Peripheral Norbornene Moieties. *Molecules* **2018**, *23*, 1007, doi:10.3390/molecules23051007.
96. Papastergiou, M.; Kanellou, A.; Chriti, D.; Raptopoulos, G.; Paraskevopoulou, P. Poly(Urethane-Acrylate) Aerogels via Radical Polymerization of Dendritic Urethane-Acrylate Monomers. *Materials* **2018**, *11*, 2249, doi:10.3390/ma11112249.
97. Papastergiou, M.; Chriti, D.; Damalas, D.E.; Raptopoulos, G.; Paraskevopoulou, P. Poly(Urethane-Acrylate) Aerogels from the Isocyanurate Trimer of Isophorone Diisocyanate. *The Journal of Supercritical Fluids* **2019**, *148*, 42–54, doi:10.1016/j.supflu.2019.02.020.
98. Taghvaee, T.; Donthula, S.; Rewatkar, P.M.; Majedi Far, H.; Sotiriou-Leventis, C.; Leventis, N. K-Index: A Descriptor, Predictor, and Correlator of Complex Nanomorphology to Other Material Properties. *ACS Nano* **2019**, *13*, 3677–3690, doi:10.1021/acsnano.9b00396.
99. Antonietti, M.; Fechler, N.; Fellinger, T.-P. Carbon Aerogels and Monoliths: Control of Porosity and Nanoarchitecture via Sol–Gel Routes. *Chem. Mater.* **2014**, *26*, 196–210, doi:10.1021/cm402239e.
100. Leventis, N. Polyurea Aerogels: Synthesis, Material Properties, and Applications. *Polymers* **2022**, *14*, 969, doi:10.3390/polym14050969.
101. Chidambareswarapattar, C.; Larimore, Z.; Sotiriou-Leventis, C.; Mang, J.T.; Leventis, N. One-Step Room-Temperature Synthesis of Fibrous Polyimide Aerogels from Anhydrides and Isocyanates and Conversion to Isomorphic Carbons. *Journal of Materials Chemistry* **2010**, *20*, 9666, doi:10.1039/c0jm01844a.

102. Leventis, N.; Sotiriou-Leventis, C.; Chandrasekaran, N.; Mulik, S.; Larimore, Z.J.; Lu, H.; Churu, G.; Mang, J.T. Multifunctional Polyurea Aerogels from Isocyanates and Water. A Structure−Property Case Study. *Chem. Mater.* **2010**, *22*, 6692–6710, doi:10.1021/cm102891d.
103. Chidambareswarapattar, C.; McCarver, P.M.; Luo, H.; Lu, H.; Sotiriou-Leventis, C.; Leventis, N. Fractal Multiscale Nanoporous Polyurethanes: Flexible to Extremely Rigid Aerogels from Multifunctional Small Molecules. *Chem. Mater.* **2013**, *25*, 3205–3224, doi:10.1021/cm401623h.
104. Leventis, N.; Chidambareswarapattar, C.; Bang, A.; Sotiriou-Leventis, C. Cocoon-in-Web-Like Superhydrophobic Aerogels from Hydrophilic Polyurea and Use in Environmental Remediation. *ACS Applied Materials & Interfaces* **2014**, *6*, 6872–6882, doi:10.1021/am500685k.
105. Bang, A.; Mohite, D.; Saeed, A.M.; Leventis, N.; Sotiriou-Leventis, C. Polydicyclopentadiene Aerogels from First- versus Second-Generation Grubbs' Catalysts: A Molecular versus a Nanoscopic Perspective. *J Sol-Gel Sci Technol* **2015**, *75*, 460–474, doi:10.1007/s10971-015-3718-0.
106. Meyers, F. IUPAC Announces the 2022 Top Ten Emerging Technologies in Chemistry Available online: https://iupac.org/iupac-2022-top-ten/ (accessed on 13 November 2022).
107. Lavoine, N.; Bergström, L. Nanocellulose-Based Foams and Aerogels: Processing, Properties, and Applications. *J. Mater. Chem. A* **2017**, *5*, 16105–16117, doi:10.1039/C7TA02807E.
108. Akimov, Yu.K. Fields of Application of Aerogels (Review). *Instruments and Experimental Techniques* **2003**, *46*, 287–299, doi:10.1023/A:1024401803057.
109. Baetens, R.; Jelle, B.P.; Gustavsen, A. Aerogel Insulation for Building Applications: A State-of-the-Art Review. *Energy and Buildings* **2011**, *43*, 761–769, doi:10.1016/j.enbuild.2010.12.012.
110. Koebel, M.; Rigacci, A.; Achard, P. Aerogel-Based Thermal Superinsulation: An Overview. *J Sol-Gel Sci Technol* **2012**, *63*, 315–339, doi:10.1007/s10971-012-2792-9.
111. Cuce, E.; Cuce, P.M.; Wood, C.J.; Riffat, S.B. Toward Aerogel Based Thermal Superinsulation in Buildings: A Comprehensive Review. *Renewable and Sustainable Energy Reviews* **2014**, *34*, 273–299, doi:10.1016/j.rser.2014.03.017.
112. Zhao, S.; Malfait, W.J.; Guerrero-Alburquerque, N.; Koebel, M.M.; Nyström, G. Biopolymer Aerogels and Foams: Chemistry, Properties, and Applications. *Angewandte Chemie International Edition* **2018**, *57*, 7580–7608, doi:10.1002/anie.201709014.
113. Villasmil, W.; Fischer, L.J.; Worlitschek, J. A Review and Evaluation of Thermal Insulation Materials and Methods for Thermal Energy Storage Systems. *Renewable and Sustainable Energy Reviews* **2019**, *103*, 71–84, doi:10.1016/j.rser.2018.12.040.
114. Linhares, T.; Amorim, M.T.P. de; Durães, L. Silica Aerogel Composites with Embedded Fibres: A Review on Their Preparation, Properties and Applications. *J. Mater. Chem. A* **2019**, *7*, 22768–22802, doi:10.1039/C9TA04811A.
115. Jones, S.M. Aerogel: Space Exploration Applications. *J Sol-Gel Sci Technol* **2006**, *40*, 351–357, doi:10.1007/s10971-006-7762-7.
116. Economopoulos, E.; Ioannides, T. Synthesis of Transparent Silica Aerogels Using Tetraalkylammonium Fluoride Catalysts. *J Sol-Gel Sci Technol* **2009**, *49*, 347–354, doi:10.1007/s10971-008-1878-x.
117. Mandal, C.; Donthula, S.; Soni, R.; Bertino, M.; Sotiriou-Leventis, C.; Leventis, N. Light Scattering and Haze in TMOS-Co-APTES Silica Aerogels. *J Sol-Gel Sci Technol* **2019**, *90*, 127–139, doi:10.1007/s10971-018-4801-0.
118. Mandal, C.; Donthula, S.; Far, H.M.; Saeed, A.M.; Sotiriou-Leventis, C.; Leventis, N. Transparent, Mechanically Strong, Thermally Insulating Cross-Linked Silica Aerogels for Energy-Efficient Windows. *J Sol-Gel Sci Technol* **2019**, *92*, 84–100, doi:10.1007/s10971-019-05100-5.
119. Biener, J.; Stadermann, M.; Suss, M.; Worsley, M.A.; Biener, M.M.; Rose, K.A.; Baumann, T.F. Advanced Carbon Aerogels for Energy Applications. *Energy Environ. Sci.* **2011**, *4*, 656–667, doi:10.1039/C0EE00627K.
120. Li, F.; Xie, L.; Sun, G.; Kong, Q.; Su, F.; Cao, Y.; Wei, J.; Ahmad, A.; Guo, X.; Chen, C.-M. Resorcinol-Formaldehyde Based Carbon Aerogel: Preparation, Structure and Applications in Energy Storage Devices. *Microporous and Mesoporous Materials* **2019**, *279*, 293–315, doi:10.1016/j.micromeso.2018.12.007.
121. Li, F.; Xie, L.; Sun, G.; Kong, Q.; Su, F.; Cao, Y.; Wei, J.; Ahmad, A.; Guo, X.; Chen, C.-M. Resorcinol-Formaldehyde Based Carbon Aerogel: Preparation, Structure and Applications in Energy Storage Devices. *Microporous and Mesoporous Materials* **2019**, *279*, 293–315, doi:10.1016/j.micromeso.2018.12.007.
122. Amonette, J.E.; Matyáš, J. Functionalized Silica Aerogels for Gas-Phase Purification, Sensing, and Catalysis: A Review. *Microporous and Mesoporous Materials* **2017**, *250*, 100–119, doi:10.1016/j.micromeso.2017.04.055.
123. Keshavarz, L.; Ghaani, M.R.; MacElroy, J.M.D.; English, N.J. A Comprehensive Review on the Application of Aerogels in CO2-Adsorption: Materials and Characterisation. *Chemical Engineering Journal* **2021**, *412*, 128604, doi:10.1016/j.cej.2021.128604.
124. Karami, D. A Review of Aerogel Applications in Adsorption and Catalysis. *Journal of Petroleum Science and Technology* **2018**, *8*, 3–15, doi:10.22078/jpst.2018.3348.1535.
125. Saeed, A.M.; Rewatkar, P.M.; Majedi Far, H.; Taghvaee, T.; Donthula, S.; Mandal, C.; Sotiriou-Leventis, C.; Leventis, N. Selective CO_2 Sequestration with Monolithic Bimodal Micro/Macroporous Carbon Aerogels Derived from Stepwise Pyrolytic Decomposition of Polyamide-Polyimide-Polyurea Random Copolymers. *ACS Appl. Mater. Interfaces* **2017**, *9*, 13520–13536, doi:10.1021/acsami.7b01910.
126. Donthula, S.; Mandal, C.; Leventis, T.; Schisler, J.; Saeed, A.M.; Sotiriou-Leventis, C.; Leventis, N. Shape Memory Superelastic Poly(Isocyanurate-Urethane) Aerogels (PIR-PUR) for Deployable Panels and Biomimetic Applications. *Chem. Mater.* **2017**, *29*, 4461–4477, doi:10.1021/acs.chemmater.7b01020.

127. Donthula, S.; Mandal, C.; Schisler, J.; Leventis, T.; Meador, M.A.B.; Sotiriou-Leventis, C.; Leventis, N. Nanostructure-Dependent Marcus-Type Correlation of the Shape Recovery Rate and the Young's Modulus in Shape Memory Polymer Aerogels. *ACS Appl. Mater. Interfaces* **2018**, *10*, 23321–23334, doi:10.1021/acsami.8b06234.
128. Chriti, D.; Raptopoulos, G.; Brandenburg, B.; Paraskevopoulou, P. Large, Rapid Swelling of High-Cis Polydicyclopentadiene Aerogels Suitable for Solvent-Responsive Actuators. *Polymers* **2020**, *12*, 1033, doi:10.3390/polym12051033.
129. Pierre, A.C.; Pajonk, G.M. Chemistry of Aerogels and Their Applications. *Chem. Rev.* **2002**, *102*, 4243–4266, doi:10.1021/cr0101306.
130. Moreno-Castilla, C.; Maldonado-Hódar, F.J. Carbon Aerogels for Catalysis Applications: An Overview. *Carbon* **2005**, *43*, 455–465, doi:10.1016/j.carbon.2004.10.022.
131. Wan, W.; Zhang, R.; Ma, M.; Zhou, Y. Monolithic Aerogel Photocatalysts: A Review. *J. Mater. Chem. A* **2018**, *6*, 754–775, doi:10.1039/C7TA09227J.
132. Maleki, H.; Hüsing, N. Current Status, Opportunities and Challenges in Catalytic and Photocatalytic Applications of Aerogels: Environmental Protection Aspects. *Applied Catalysis B: Environmental* **2018**, *221*, 530–555, doi:10.1016/j.apcatb.2017.08.012.
133. Saeed, A.M.; Wisner, C.A.; Donthula, S.; Majedi Far, H.; Sotiriou-Leventis, C.; Leventis, N. Reuseable Monolithic Nanoporous Graphite-Supported Nanocatalysts (Fe, Au, Pt, Pd, Ni, and Rh) from Pyrolysis and Galvanic Transmetalation of Ferrocene-Based Polyamide Aerogels. *Chem. Mater.* **2016**, *28*, 4867–4877, doi:10.1021/acs.chemmater.6b02364.
134. García-González, C.A.; Budtova, T.; Durães, L.; Erkey, C.; Del Gaudio, P.; Gurikov, P.; Koebel, M.; Liebner, F.; Neagu, M.; Smirnova, I. An Opinion Paper on Aerogels for Biomedical and Environmental Applications. *Molecules* **2019**, *24*, 1815, doi:10.3390/molecules24091815.
135. Kaya, G.G.; Aznar, E.; Deveci, H.; Martínez-Máñez, R. Aerogels as Promising Materials for Antibacterial Applications: A Mini-Review. *Biomater. Sci.* **2021**, *9*, 7034–7048, doi:10.1039/D1BM01147B.
136. Mikkonen, K.S.; Parikka, K.; Ghafar, A.; Tenkanen, M. Prospects of Polysaccharide Aerogels as Modern Advanced Food Materials. *Trends in Food Science & Technology* **2013**, *34*, 124–136, doi:10.1016/j.tifs.2013.10.003.
137. Maleki, H. Recent Advances in Aerogels for Environmental Remediation Applications: A Review. *Chemical Engineering Journal* **2016**, *300*, 98–118, doi:10.1016/j.cej.2016.04.098.
138. Kumar, A.; Rana, A.; Sharma, G.; Sharma, S.; Naushad, Mu.; Mola, G.T.; Dhiman, P.; Stadler, F.J. Aerogels and Metal–Organic Frameworks for Environmental Remediation and Energy Production. *Environ Chem Lett* **2018**, *16*, 797–820, doi:10.1007/s10311-018-0723-x.
139. AERoGELS COST Action Available online: https://cost-aerogels.eu/ (accessed on 13 November 2022).
140. Konstantinou, M.; Pashalidis, I. Speciation and Spectrophotometric Determination of Uranium in Seawater. *Mediterranean Marine Science* **2004**, *5*, 55–60, doi:10.12681/mms.210.
141. Paraskevopoulou, P.; Smirnova, I.; Athamneh, T.; Papastergiou, M.; Chriti, D.; Mali, G.; Čendak, T.; Chatzichristidi, M.; Raptopoulos, G.; Gurikov, P. Mechanically Strong Polyurea/Polyurethane-Cross-Linked Alginate Aerogels. *ACS Appl. Polym. Mater.* **2020**, *2*, 1974–1988, doi:10.1021/acsapm.0c00162.
142. Paraskevopoulou, P.; Smirnova, I.; Athamneh, T.; Papastergiou, M.; Chriti, D.; Mali, G.; Čendak, T.; Raptopoulos, G.; Gurikov, P. Polyurea-Crosslinked Biopolymer Aerogel Beads. *RSC Advances* **2020**, *10*, 40843, doi:https://doi.org/10.1039/D0RA07337G.
143. Fricke, M.; Paraskevopoulou, P.; Gurikov, P.; Chriti, D.; Papastergiou, M.; Raptopoulos, G.; Athamneh, T.; Smirnova, I.; Movahed, S.; Weinrich, D.; Loesberg, W. Polyurea/Polyurethane-Crosslinked Alginate Aerogels, EP3848409A1 2021.
144. Raptopoulos, G.; Papastergiou, M.; Chriti, D.; Effraimopoulou, E.; Čendak, T.; Samartzis, N.; Mali, G.; Ioannides, T.; Gurikov, P.; Smirnova, I.; Paraskevopoulou, P. Metal-Doped Carbons from Polyurea-Crosslinked Alginate Aerogel Beads. *Mater. Adv.* **2021**, *2*, 2684–2699, doi:10.1039/D0MA01025A.
145. Paraskevopoulou, P.; Raptopoulos, G.; Leontaridou, F.; Papastergiou, M.; Sakellari, A.; Karavoltsos, S. Evaluation of Polyurea-Crosslinked Alginate Aerogels for Seawater Decontamination. *Gels* **2021**, *7*, 27, doi:10.3390/gels7010027.
146. Georgiou, E.; Pashalidis, I.; Raptopoulos, G.; Paraskevopoulou, P. Efficient Removal of Polyvalent Metal Ions (Eu(III) and Th(IV)) from Aqueous Solutions by Polyurea-Crosslinked Alginate Aerogels. *Gels* **2022**, *8*, 478, doi:10.3390/gels8080478.
147. Zoi, A.; Karanika, E.A. Heavy Metals Uptake from Water Using Polyurea-Crosslinked Alginate Aerogels, Diploma Thesis, Department of Chemistry, National and Kapodistrian University of Athens: Greece, 2021.
148. Pashalidis, I.; Czerwinski, K.R.; Fanghänel, T.; Kim, J.I. Solid-Liquid Phase Equilibria of Pu(VI) and U(VI) in Aqueous Carbonate Systems. Determination of Stability Constants. *Radiochimica Acta* **1997**, *76*, 55–62, doi:10.1524/ract.1997.76.12.55.
149. Hubbe, M.A.; Azizian, S.; Douven, S. Implications of Apparent Pseudo-Second-Order Adsorption Kinetics onto Cellulosic Materials: A Review. *BioResources* **2019**, *14*, 7582–7626.
150. Lima, E.C.; Sher, F.; Guleria, A.; Saeb, M.R.; Anastopoulos, I.; Tran, H.N.; Hosseini-Bandegharaei, A. Is One Performing the Treatment Data of Adsorption Kinetics Correctly? *Journal of Environmental Chemical Engineering* **2021**, *9*, 104813, doi:10.1016/j.jece.2020.104813.
151. Liakos, E.V.; Lazaridou, M.; Michailidou, G.; Koumentakou, I.; Lambropoulou, D.A.; Bikiaris, D.N.; Kyzas, G.Z. Chitosan Adsorbent Derivatives for Pharmaceuticals Removal from Effluents: A Review. *Macromol* **2021**, *1*, 130–154, doi:10.3390/macromol1020011.
152. Payne, T.E.; Brendler, V.; Ochs, M.; Baeyens, B.; Brown, P.L.; Davis, J.A.; Ekberg, C.; Kulik, D.A.; Lutzenkirchen, J.; Missana, T.; Tachi, Y.; Van Loon, L.R.; Altmann, S. Guidelines for Thermodynamic Sorption Modelling in the Context of Radioactive Waste Disposal. *Environmental Modelling & Software* **2013**, *42*, 143–156, doi:10.1016/j.envsoft.2013.01.002.
153. Liatsou, I.; Pashalidis, I.; Nicolaides, A. Triggering Selective Uranium Separation from Aqueous Solutions by Using Salophen-Modified Biochar Fibers. *J Radioanal Nucl Chem* **2018**, *318*, 2199–2203, doi:10.1007/s10967-018-6186-5.

154. Konstantinou, M.; Kasseta, G.; Pashalidis, I. Boron Adsorption on Alumina (Al_2O_3) and Magnesia (MgO) in Aqueous Solutions: A Comparative Study. *International Journal of Environmental Technology and Management* **2006**, *6*, 466–479, doi:10.1504/IJETM.2006.010478.
155. Chriti, D.; Raptopoulos, G.; Anyfantis, G.C.; Paraskevopoulou, P. An Extreme Case of Swelling of Mostly Cis-Polydicyclopentadiene by Selective Solvent Absorption—Application in Decontamination and Environmental Remediation. *ACS Appl. Polym. Mater.* **2019**, *1*, 1648–1659, doi:10.1021/acsapm.9b00221.